



**HAL**  
open science

## The Chemical Characteristics of Rainwater and Wet Atmospheric Deposition Fluxes at Two Urban Sites and One Rural Site in Côte d'Ivoire

Mohamed Kassamba-Diaby, Corinne Galy-Lacaux, Véronique Yoboué,  
Jonathan Hickman, Camille Mouchel-Vallon, Kerneels Jaars, Sylvain  
Gnamien, Richmond Konan, Eric Gardrat, Siélé Silué

### ► To cite this version:

Mohamed Kassamba-Diaby, Corinne Galy-Lacaux, Véronique Yoboué, Jonathan Hickman, Camille Mouchel-Vallon, et al.. The Chemical Characteristics of Rainwater and Wet Atmospheric Deposition Fluxes at Two Urban Sites and One Rural Site in Côte d'Ivoire. *Atmosphere*, 2023, 14 (5), pp.809. 10.3390/atmos14050809 . hal-04621609

**HAL Id: hal-04621609**

**<https://hal.science/hal-04621609>**

Submitted on 25 Jun 2024

**HAL** is a multi-disciplinary open access archive for the deposit and dissemination of scientific research documents, whether they are published or not. The documents may come from teaching and research institutions in France or abroad, or from public or private research centers.

L'archive ouverte pluridisciplinaire **HAL**, est destinée au dépôt et à la diffusion de documents scientifiques de niveau recherche, publiés ou non, émanant des établissements d'enseignement et de recherche français ou étrangers, des laboratoires publics ou privés.



Distributed under a Creative Commons Attribution 4.0 International License

## Article

# The Chemical Characteristics of Rainwater and Wet Atmospheric Deposition Fluxes at Two Urban Sites and One Rural Site in Côte d'Ivoire

Mohamed L. Kassamba-Diaby <sup>1,\*</sup>, Corinne Galy-Lacaux <sup>2,\*</sup>, Véronique Yoboué <sup>1</sup>, Jonathan E. Hickman <sup>3,4</sup>, Camille Mouchel-Vallon <sup>2</sup> , Kerneels Jaars <sup>5</sup> , Sylvain Gnamien <sup>1</sup>, Richmond Konan <sup>1</sup>, Eric Gardrat <sup>2</sup> and Siélé Silué <sup>6</sup>

<sup>1</sup> Laboratoire des Sciences de la Matière, de l'Environnement et de l'Énergie Solaire, Département de Physique, Unité de Formation et de Recherche en Sciences des Structures des Matières et de la Technologie, Université Félix Houphouët-Boigny, Abidjan BPV 34, Côte d'Ivoire; veronique.yoboue94@ufhb.edu.ci (V.Y.); gnamien.sylvain@ufhb.edu.ci (S.G.); konan.richmond75@ufhb.edu.ci (R.K.)

<sup>2</sup> Laboratoire d'Aérodynamique, Université Toulouse III Paul Sabatier, CNRS, 14 Avenue Édouard Belin, 31400 Toulouse, France; camille.mouchel-vallon@aero.obs-mip.fr (C.M.-V.); eric.gardrat@aero.obs-mip.fr (E.G.)

<sup>3</sup> Center for Climate Systems Research, Columbia University, 2880 Broadway, New York, NY 10025, USA; jonathan.e.hickman@nasa.gov

<sup>4</sup> NASA Goddard Institute for Space Studies, 2880 Broadway, New York, NY 10025, USA

<sup>5</sup> Atmospheric Chemistry Research Group, North-West University, Potchefstroom, 11 Hoffman Street, Potchefstroom 2531, South Africa; kerneels.jaars@nwu.ac.za

<sup>6</sup> Département de Mathématiques, Physique et Chimie, University Peloforo Gbon Coulibaly, Korhogo P.O. Box 1328, Côte d'Ivoire; sielesilue@upgc.edu.ci

\* Correspondence: diaby.kassamba22@ufhb.edu.ci (M.L.K.-D.); corinne.galy-lacaux@aero.obs-mip.fr (C.G.-L.)



**Citation:** Kassamba-Diaby, M.L.; Galy-Lacaux, C.; Yoboué, V.; Hickman, J.E.; Mouchel-Vallon, C.; Jaars, K.; Gnamien, S.; Konan, R.; Gardrat, E.; Silué, S. The Chemical Characteristics of Rainwater and Wet Atmospheric Deposition Fluxes at Two Urban Sites and One Rural Site in Côte d'Ivoire. *Atmosphere* **2023**, *14*, 809. <https://doi.org/10.3390/atmos14050809>

Academic Editors: Elena Hristova, Manousos Ioannis Manousakas, Anikó Angyal and Maria Gini

Received: 27 March 2023

Revised: 22 April 2023

Accepted: 24 April 2023

Published: 28 April 2023



**Copyright:** © 2023 by the authors. Licensee MDPI, Basel, Switzerland. This article is an open access article distributed under the terms and conditions of the Creative Commons Attribution (CC BY) license (<https://creativecommons.org/licenses/by/4.0/>).

**Abstract:** Due to their close relationship with atmospheric chemical composition and global impacts on ecosystems, it is of crucial importance to determine rain chemical composition and quantify wet deposition. In this study, we characterized the chemical composition of precipitation at one rural and two urban sites in Côte d'Ivoire along a south-north transect. Annual and monthly Volume Weighted Mean (VWM) concentration of major ions, as well as wet deposition fluxes in rainwater samples from Abidjan, Korhogo (urban sites), and Lamto (rural site), have been calculated. We also simulated air mass back-trajectories and generated satellite maps of burnt fraction and nitrogen species emissions ( $\text{NH}_3$ ,  $\text{NO}_2$ ) to better analyze our results. Results show that the dominant ion at both urban sites is  $\text{Ca}^{2+}$ , whereas  $\text{NH}_4^+$  dominates the chemical content of the Lamto rural site. The analysis of atmospheric sources of influence shows that urban sites rains are characterized by a mixture of terrigenous continental and anthropogenic sources (39–33%), as well as a high marine contribution (34–24%) and a significant nitrogenous contribution (18–25%) mainly associated to fossil fuel from road traffic, domestic and biomass burning sources. At the rural Lamto site, marine, terrigenous, and nitrogenous contributions represent, respectively, 14%, 25%, and 30%. The average pH values are, respectively, 5.76, 5.31, and 5.57 for Abidjan, Lamto, and Korhogo, with a preponderance of mineral acidity contribution at the urban sites, while the organic acidity contribution dominates in Lamto. Neutralization factor (NF) of mineral and organic acids calculations revealed that  $\text{Ca}^{2+}$  and  $\text{NH}_4^+$  are the most important neutralizing ions in the rain at all three sites, and we estimated that 79% to 87% of the rain acidity is neutralized by alkaline compounds.

**Keywords:** rainwater; chemical composition; wet deposition; acidification; neutralization; eutrophication; urban; rural sites; Côte d'Ivoire; Africa

## 1. Introduction

Atmospheric deposition represents a key mechanism in anthropogenic impacts on the environment. Atmospheric deposition includes wet and dry processes and is the major

removal pathway of atmospheric pollutants and thus contributes to the earth-atmosphere biogeochemical balance [1–4]. Limiting anthropogenic impacts on atmospheric deposition is considered fundamental for addressing several sustainable development goals, such as food security, climate change, human health, and biodiversity [3,5,6]. The study of deposition processes and the determination of deposition fluxes is important for understanding the spatial and temporal evolution of the atmosphere's chemical composition and of the biogeochemical cycles of elements such as nitrogen, carbon, and sulfur. Biogeochemical cycles are strongly affected by anthropogenic activities, and atmospheric deposition can act as a source of nutrients but also as a source of toxins [7–9].

Wet deposition plays a key role in removing both gaseous and particulate pollutants from the atmosphere and thus influences atmospheric chemistry [7,8]. Rain chemical composition provides insights into the evolution of the chemical atmosphere composition, and it is influenced by numerous factors, including the type and strength of natural/anthropogenic sources of atmospheric compounds, long-range transport, the origin of continental air masses, as well as removal processes related to the intensity and temporal distribution of rainfall patterns [2,9,10]. Investigation of rainwater chemistry at a regional representative urban site in southern India revealed that the ionic composition of rainwater in the region is more influenced by terrestrial sources than anthropogenic and marine sources [11]. Rainwater samples were collected at five locations in the Pune region, an urban area in the southwestern part of India, from 2006 to 2009 [12]. The chemical analysis of these samples demonstrated the strong contribution of soil dust as well as an influence from marine and anthropogenic sources in that area. A long-term analysis of European precipitations from 2000 to 2017 [10] showed that the rainwater composition is mostly controlled by anthropogenic sources. Therefore rainfall composition is useful for understanding the direct impacts of air pollution on ecosystems and is also an important indicator in the determination of pollution levels in urban areas [11–13]. Lack of accurate descriptions of deposition processes and thorough evaluation with high-quality measurements remain major weaknesses of global deposition modeling. This is particularly true in tropical regions, which are often affected by a convective rainfall regime and where long-term, high-quality data on deposition are scarce [2,3,6].

In this context, the most recent study is the global assessment of precipitation chemistry and deposition carried out under the auspices of the World Meteorological Organization (WMO)—Global Atmospheric Watch (GAW) program, Geneva, Switzerland [2]. The conclusion of that assessment led to some recommendations to address major gaps and uncertainties in global ion concentrations and deposition measurements. One of these recommendations emphasizes the lack of measurements in tropical regions and the weakness of the spatial coverage in different continents such as South America, parts of India, and Africa [2,3].

The assessment recognized the importance of the unique long-term quality-controlled database in Africa provided by the International Network to study Deposition and Atmospheric chemistry in Africa (INDAAF, <https://indaaf.obs-mip.fr> (accessed on 26 April 2023) even though the number of measurement stations remains low. The INDAAF program, initiated in 1994, aims to study atmospheric composition and wet and dry deposition fluxes in Africa.

Many syntheses studies representative of rural sites along an eco-systemic transect (dry savannas, wet savannas, forests) have been published [1,8,9,14,15]. These works have characterized precipitation chemistry and deposition in African rural areas, but, to our knowledge, few studies consider African urban areas. In the context of the rapid urbanization and demographic explosion in Africa, especially in Côte d'Ivoire, where the percentage of the national population living in urban areas is expected to increase to 60% by 2025 and exceed 70% by 2050 [16], it is important to improve the understanding of urban atmospheric composition and the potential impacts of air pollution on developing countries' megacities [17].

The present study proposes to establish the characteristics of the chemical composition of precipitation and the deposition fluxes of two urban areas and one rural area in Côte d'Ivoire, together representative of a continental south-north transect. This work was

carried out within the framework of the Air Pollution and Health in Urban Areas program (PASMU) implemented in 2018 and the INDAAF program. The goals of this study are: (1) to document a three-year time period (2018–2020) the rainwater chemical composition and the deposition fluxes of soluble ions, including concentrations of major ions, variation of pH, concentrations of sea salts, neutralizing capacity of precipitation, and ion enrichment factors, (2) to provide a better understanding of ion sources contribution and the climatology that influence annual, seasonal and monthly precipitation content. This study offers a baseline record for urban sites in African cities against which future changes in emissions and potential environmental impacts can be evaluated and responds to international recommendations that emphasize the scarcity of deposition measurements on the African continent, recognized at a global scale to be a continent faced with major environmental sustainability issues [18,19].

## 2. Materials and Methods

### 2.1. Sites Description

This study considers three measurement sites, two urban and one rural, located along a south-north transect in Côte d'Ivoire (Figure 1). The two urban sites, Abidjan and Korhogo, have been selected and studied in the framework of the PASMU program and are, respectively, located in the south and north of Côte d'Ivoire. The modes of transportation, the types of fuel used by households, and the population density make it possible to distinguish and characterize both of these urban sites. In Côte d'Ivoire, southern cities are generally more populated and industrialized than those in the north, as Abidjan's population is 10 times larger than Korhogo's [20].

The first urban site is located in Abidjan ( $5^{\circ}20'43''$  N;  $4^{\circ}1'27''$  W), which is a metropolitan area on the south-east coast of Côte d'Ivoire and considered to be the economic capital of the country, Abidjan is the largest city in Côte d'Ivoire with a population over 4,707,404, which is approximately 20% of the entire country's population, and a surface area of 2119 km<sup>2</sup> [21]. This city is an autonomous district divided into 13 districts. The sampling site was on the rooftop of the Institut de Recherche et de Développement (IRD) building (Figure 1), which is in the suburb of Cocody, in the vicinity of the University Felix Houphouët Boigny. Major pollution sources in the city are fossil fuel combustion from the traffic of motorized vehicles, residential coal burning, open waste burning, and some emissions from industrial activities flaring [20,22]. Ref. [23] estimated that the national fleet of vehicles was 636,551 in 2016, with 80% of them in Abidjan (498,531 vehicles).

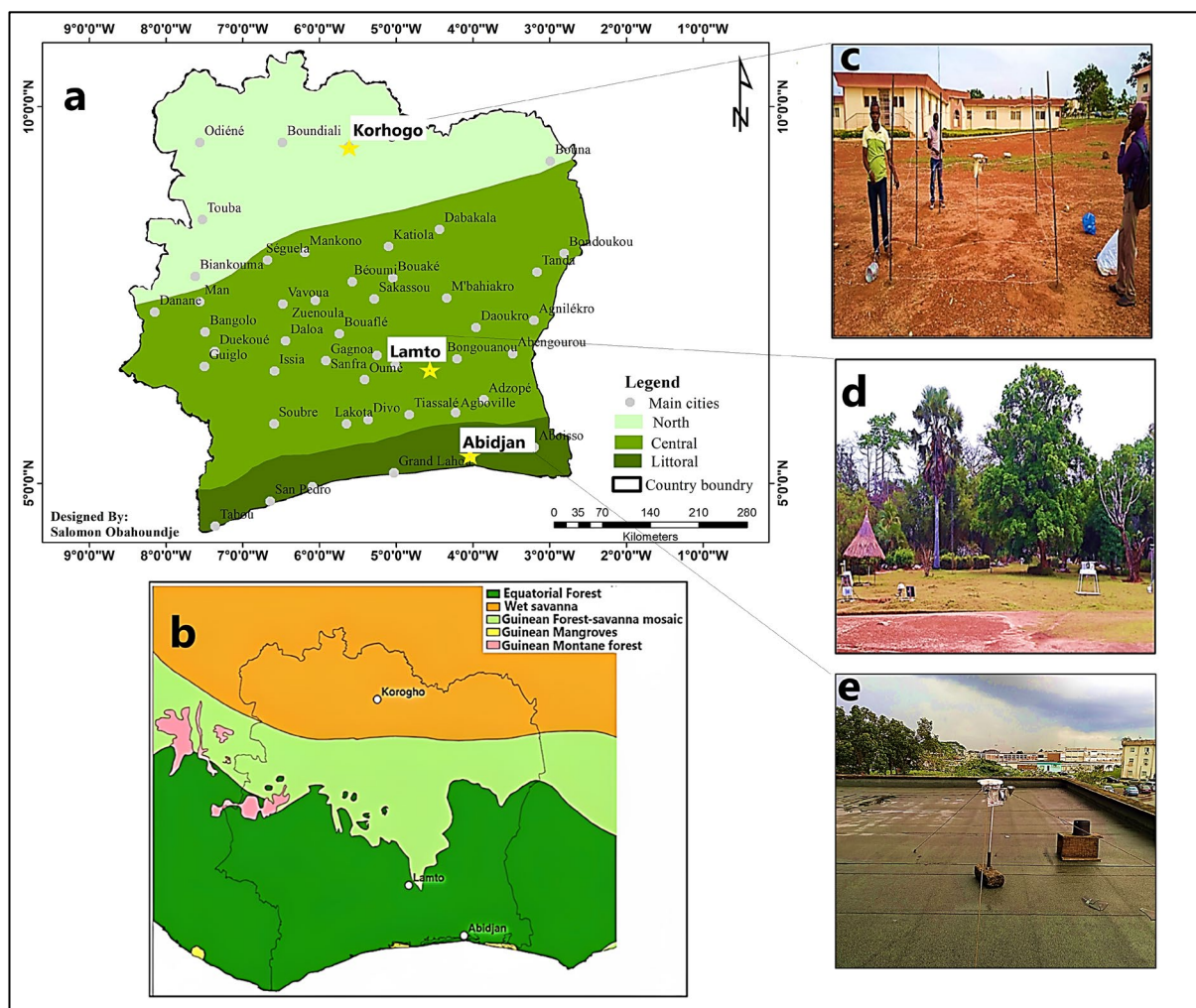


**Figure 1.** Locations of the three measurement sites on the Abidjan-Lamto-Korhogo transect: (a) map of climatic subdivision in Côte d'Ivoire adapted from [24]; (b) map of ecoregions subdivision in Côte d'Ivoire; (c) Korhogo; (d) Lamto; (e) Abidjan.

The second urban site is located in the city of Korhogo (9°28' N; 5°36'51" W), which is situated in the north of Côte d'Ivoire, approximately 635 km from Abidjan in the savannas district (Figure 1c). Korhogo is spread over an area of 12.50 km<sup>2</sup> and has a population of 243,048 inhabitants, according to the last population census in 2014 [21]. Korhogo is strongly influenced by agricultural activities, even though it is an urban area. According to [25], Korhogo is the epicenter of the cotton and cashew culture boom, which is dependent on fertilizers and pesticides for crop production. Considering urbanization and industrialization, Korhogo is far from the level of megacities such as Abidjan, although it has recorded substantial population growth since the political crisis in 2002, resulting in an increase of the city area from 3300 ha in 2000 to 10,000 ha in 2019 [26]. The mode of transport is dominated by two-wheeled vehicles. This trend is also observed at the level of public transport with the emergence of motorcycle cabs, "Taxi-motos", which constitute one of the main means of transportation since the prohibition of four-wheeled taxi vehicles [27].

The third sampling site, Lamto, represents a super-site of the INDAAF project and is located in the central part of the country, at the tip of the "V Baoule", which represents an ecological zone of transition between the forest and the savanna ecosystem (Figure 1d). Lamto (6°13' N, 5°02' W) is located in the Agnéby-Tiassa region, in the Tiassalé department, about 165 km north-west of Abidjan and 433 km south-east of Korhogo. It is in a natural reserve that covers approximately 2600 ha and is representative of a soudano-guinean wet savanna with the so-called gallery forest along the Bandama River [28].

### 2.2. Meteorological Quantities

Meteorological quantities from 2018 to 2020 (monthly temperature and relative humidity) were provided by the SODEXAM (Society of Exploitation and Airport Development, Aeronautics, and Meteorology) for Abidjan and Korhogo, as well as long-term rainfall databases for the periods 1980–2020 and 1990–2020, respectively. From 2018 to 2020 in Abidjan, we used rainfall data measured by the EVIDENCE project (Extreme rainfall events, vulnerability to flooding, and water contamination), and data are available at the following address: <http://www.evidence-ci.org/> (accessed on 26 April 2023). The project has installed a rain gauge collocated with the rain sampler. It is composed of a tipping bucket rain gauge (0.5 mm tilting of the bucket) and a Précis Mécanique® (rain interception cone 1.5 m from the ground and with a surface area equal to 400 cm<sup>2</sup>). Tipping bucket dates (day, month, year, hour, minute, second) are recorded in a HOBO Pendant® UA-003-64 data logger. In Korhogo, we used rainfall data reported by the SODEXAM. The rain gauge data were collected monthly. At the Lamto site, the INDAAF long-term monitoring program provides air temperature, humidity, and rainfall data for the studied period [29].

### 2.3. Sample Collection

Precipitation sampling at the three sites was performed using a semi-automatic collector of precipitation designed for the INDAAF network (<http://indaaf.obs-mip.fr> (accessed on 26 April 2023)). The instrument, as well as the sampling protocols, have been fully described in several studies [1,8,9].

The rain sampling protocol follows the WMO/GAW international standards recommendations [30]. After collection, samples are stored in a freezer to stop any chemical reaction and sent for analysis at the Laboratoire d’Aerologie (LAERO) in Toulouse (France). Chemical analysis is performed no later than 6 months after sampling. Table 1 presents the annual total precipitation (Pt) in mm, the percent total precipitation (%TP), and the interannual variability as a percentage relative to the mean annual rainfall for the 1980–2020 period, 1998–2020 period, and 1990–2020 period, respectively, for Abidjan, Lamto, and Korhogo.

**Table 1.** Rainwater collection at Abidjan, Lamto, and Korhogo (2018–2020): Annual Total Precipitation (Pt, mm), Interannual variability (%), Collected precipitation (Pc, mm), and Number of collected rain events (Nc), Percent total precipitation (%TP), Annual percent coverage length (%PCL) and in brackets: %PCL for each quarter (0 and 1 mean 0% and 100%, respectively).

Sites	Abidjan			Lamto			Korhogo		
	Year	2018	2019	2020	2018	2019	2020	2018	2019
Pt (mm)	1477.7	1355.4	1593.7	1090.9	1508.2	1101.4	1160.7	1162.5	1083
Interannual Variability (%)	−2.91	−10.94	4.71	−0.80	22.71	−10.38	−2.21	−2.06	−8.76
Pc (mm)	825	1006.20	1288.30	1077.60	1459.40	988	745.55	862.80	783.10
(Nc)	(56)	(81)	(84)	(91)	(70)	(78)	(48)	(52)	(43)
%TP (%)	56	74	81	99	97	90	64	74	72
Annual %PCL (%)	75	100	100	100	100	100	75	100	100
(quarterly)	(0,1,1,1)	(1,1,1,1)	(1,1,1,1)	(1,1,1,1)	(1,1,1,1)	(1,1,1,1)	(0,1,1,1)	(1,1,1,1)	(1,1,1,1)

As defined by [30], (%TP) is the ratio between annual precipitation (Pt) and collected precipitation (Pc). Annual and quarterly Percent Coverage Length (%PCL) is an indicator of the representativity of the sampled period. From April 2018 to December 2020 in Abidjan, the total and collected rainfall were 4426.8 mm and 3119.5 mm, respectively, with a total of 221 collected rain samples. In Lamto, from January 2018 to December 2020, the total and collected rainfall were 3700.5 mm and 3525 mm, respectively, with a total of 239 rain samples. In Korhogo, from May 2018 to December 2020, the total and collected rainfall was 3406.2 mm and 2391.45 mm, respectively, with a total of 143 rain samples.

The %TP shows that rainwater collection is not representative of 2018 in Abidjan and Korhogo (56% and 64%, respectively). Lamto presents a good collection representing all the years (%TP 90–99%). In reference to the WMO international standards, we assume that precipitation collection at Abidjan, Lamto, and Korhogo in 2019 and 2020 can be considered

representative of the studied period (PCL = 100%) (Table 1). Annual volume weighted mean (VWM) and Wet deposition fluxes (WD) will be thus calculated only for 2019, 2020, and the mean period 2019–2020. Data from January 2018 to December 2020 will be used to calculate monthly Volume Weighted Mean (VWM) and Wet Deposition (WD) according to the quarterly %PCL (Table 1).

#### 2.4. Analytical Procedures and Quality Assurance/Quality Control

Major inorganic ( $\text{Na}^+$ ,  $\text{K}^+$ ,  $\text{Mg}^{2+}$ ,  $\text{Ca}^{2+}$ ,  $\text{Cl}^-$ ,  $\text{NO}_3^-$ ,  $\text{SO}_4^{2-}$ ,  $\text{NH}_4^+$ ) and organic carboxylic acids ions ( $\text{HCOO}^-$ ,  $\text{CH}_3\text{COO}^-$ ,  $\text{C}_2\text{H}_5\text{COO}^-$ ,  $\text{C}_2\text{O}_4^{2-}$ ) were determined by Ionic Chromatography (IC) as described in [9,14]. The IC analysis is performed using a Thermo ICS5000+ and an ICS 1100 Ionic chromatograph with two automated samplers (AS50) (Thermo Fisher Scientific, Waltham, MA, USA). The eluents for anions and cations are NaOH and MSA (methanesulfonic acid), respectively. Certified ionic standards from SCP SCIENCE are used for IC calibration. pH is measured with an ATI Orion 350 pH-meter with a combined electrode (ATI Orion model 9252) (Thermo Electron Corporation, Horsham, UK) filled with KCl (4 M) and saturated with AgCl. Two standard solutions (WTW) at pH 4.01 and 7.00 are used for its calibration. The precision is 0.01 pH unit.

Data quality is further ensured by calculating the ionic balance [30]. Analyses were performed on 221 rain samples collected in Abidjan, 239 rain samples collected in Lamto, and 143 rain samples collected in Korhogo (Table 1). Results indicate that 94, 98, and 89% of the rain samples collected in Abidjan, Lamto, and Korhogo, respectively, are in the WMO acceptance range and will be considered in all the calculations presented in the result sections.

#### 2.5. Satellite Data

We used version 1.6 of the CrIS-Fast Physical Retrieval (CFPR)- $\text{NH}_3$  satellite product [31,32]. The product compares well with in situ and ground-based FTIR observations. For this study, only daytime observations from 2018 to 2020 are used. Note that observations for April–July 2019 are not available due to instrument errors. We used level 3 (L3) data at  $0.25^\circ \times 0.25^\circ$  resolution from the NASA tropospheric  $\text{NO}_2$  standard product from the Ozone Monitoring Instrument (OMI) (Dutch Space and TNO Science & Industry (formerly TNO-TPD) in The Netherlands, in co-operation with Finnish subcontractors VTT and Patria Finavitec, Netherlands). OMI is a nadir-viewing spectrometer in a sun-synchronous orbit with near-daily global coverage that measures solar backscatter in the UV-visible range [33]. For our analyses of satellite retrievals over Abidjan, Lamto, and Korhogo, we selected observations centered around the  $0.25^\circ$  grid cell containing each site to create a  $1^\circ$  field of  $\text{NO}_2$  or  $\text{NH}_3$  Vertical Column Densities (VCDs). The average over this  $1^\circ$  grid cell was used as an estimate of VCDs over the site.

#### 2.6. Calculations and Statistics

Volume Weighted Mean (VWM) concentrations in  $\mu\text{eq L}^{-1}$ , Wet Deposition fluxes (WD) for all ionic species in  $\text{kg ha}^{-1} \text{yr}^{-1}$ , Sea Salt Fraction (SSF) and Non-Sea Salt Fraction (NSSF) to ionic concentrations, potential Acidity (pA), Fractional Acidity (FA) and the Neutralization Factor (NF) were calculated using Equations (S1)–(S10) presented in the Supplementary Materials (S4).

#### 2.7. Back Trajectories

In order to determine the impact of air masses on the chemical composition of collected rainwater samples, the air mass trajectories history for each site for the entire sampling period was determined by calculating back trajectories with the Hybrid Single-Particle Lagrangian Integrated Trajectory (HYSPLIT) model (version 4.8, [34]) using the National Weather Service's (NWS) National Centers for Environmental Prediction model data (NCEP, available at [www.ready.noaa.gov/archives.php](http://www.ready.noaa.gov/archives.php) (accessed on 26 April 2023)). Hourly-arriving 96-h back trajectories were calculated at three arrival heights, 100, 1500, and 2500 m, respectively, above ground level. These individual back trajectories were then

superimposed, in order to generate monthly or seasonal overlay back trajectories for the study period, on a frequency map with a  $0.2^\circ \times 0.2^\circ$  resolution grid to show the statistical distribution [35].

### 3. Results and Discussion

#### 3.1. Sites Climatology

The West African climate is highly dependent on the Intertropical Convergence Zone (ITCZ) position, which is the limit between a cool and humid marine air mass (Monsoon) and a warm and dry Saharan air mass (Harmattan). This climate is largely influenced by the ITCZ variability at the regional scale in Côte d'Ivoire. Indeed, the extreme latitudinal positions of ITCZ in January ( $5^\circ\text{N}$ ) and in August ( $22^\circ\text{N}$ ) divide the country into three distinct climatic zones: the Northern, the Central, and the Coastal Climatic zones [36] (Figure 1a). Abidjan, Lamto, and Korhogo are located, respectively, in the coastal, central, and northern climatic zones, and pluviometric regimes depend on the climatic zones [37].

Abidjan is characterized by a bimodal rainfall regime defined by two wet seasons and two dry seasons. A long-wet season that lasts from March to July and a short-wet season from October to November. The long dry season lasts from December to February, and the short dry season from August to September (Figure 2c) [38]. Abidjan is characterized by a first rainfall maximum in May and a second in October (Figure 2c).

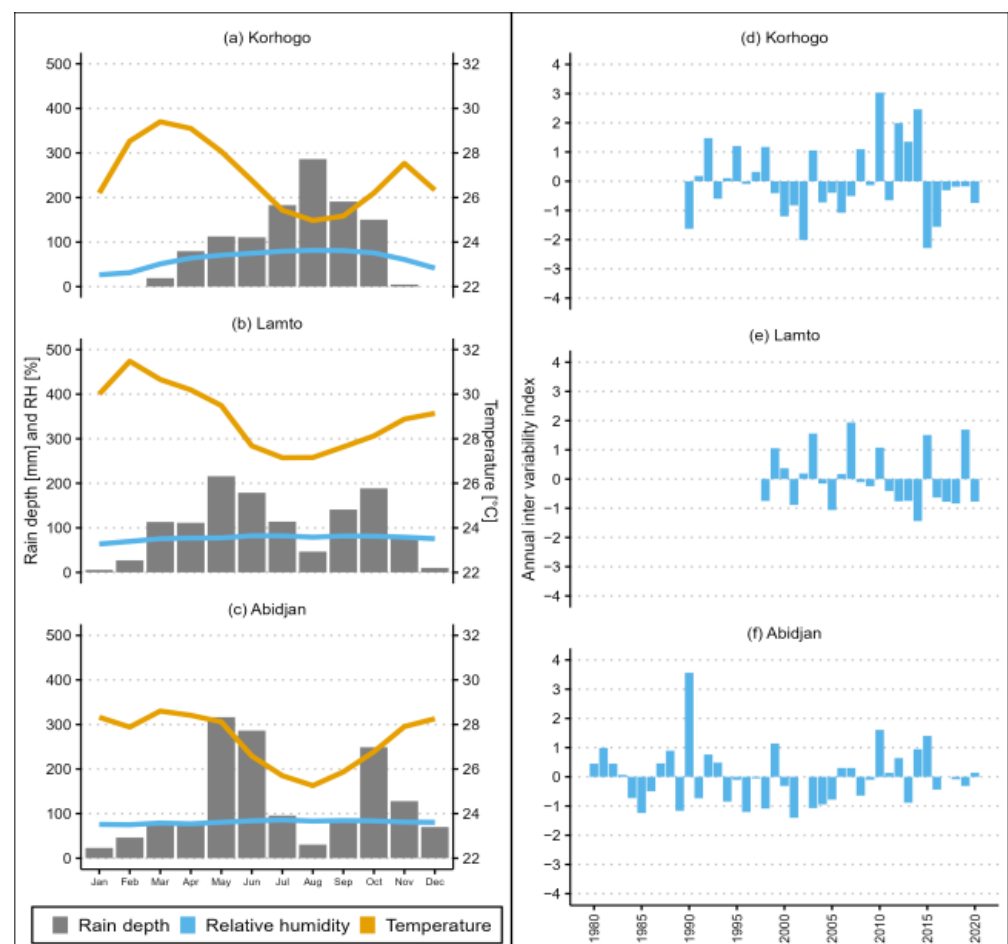


**Figure 2.** Monthly mean meteorological parameters measured at (a) Korhogo, (b) Lamto, and (c) Abidjan (2018–2020) (Air temperature ( $^\circ\text{C}$ ), Relative Humidity (0–100%), Rain depth (mm), note secondary axis for temperature); Annual Inter variability Index (AII) for (d) Korhogo (1990–2020), (e) Lamto (1998–2020) and (f) Abidjan (1980–2020).

Lamto has a mild, warm, and wet climate. We also distinguish two wet seasons and two dry seasons: a long wet season extends from March to July, mainly influenced by monsoon air masses, and a long dry season from December to February, influenced by the Saharan air masses (harmattan) [29]. The short dry and wet seasons are limited to the month of August and from September to November, respectively (Figure 2b). Korhogo is characterized by a unimodal rainfall regime with a single wet season from April to October and a single dry season from November to March (Figure 2a). Korhogo belongs to the tropical regime of transition, characterized by a maximum rainfall in August.

Annual mean air temperature and relative humidity over the study period in the transect Abidjan-Lamto-Korhogo are, respectively,  $27.30 \pm 1.10$  °C and  $80 \pm 3.89\%$ ,  $28.98 \pm 1.10$  °C and  $77.05 \pm 5.53\%$  and  $27.00 \pm 0.08$  °C and  $60 \pm 0.81\%$  (Figure 2a–c). Temperature ranged from  $25.3 \pm 0.20$  °C in August to  $28.65 \pm 1.85$  °C in March, from  $27.15 \pm 0.21$  °C in August to  $31.48 \pm 0.25$  °C in February, and from  $25.2 \pm 0.30$  °C in August to  $29.50 \pm 0.26$  °C in April, respectively, in Abidjan, Lamto, and Korhogo (Figure 2a–c).

The rainfall Annual Inter variability Index (AII) is defined as:

$$AII = (P_i - P_m) / \sigma, \quad (1)$$

$P_i$  (mm) is the cumulative rainfall for a year,  $P_m$  (mm) and  $\sigma$  are, respectively, the mean and the standard deviation of the annual rainfall observed for a given series. This index allows for characterizing the general patterns of precipitation over the study period [39] (Figure 2). The degree of drought is a function of the precipitation index (AII). Index intermediate values are classified as follows: high humidity ( $1 < AII < 2$ ), moderate humidity ( $0 < AII < 1$ ), moderate drought ( $-1 < AII < 0$ ), and strong drought ( $-2 < AII < -1$ ).

The AII index calculation based on the annual rainfall database ranged from 784 mm in 2001 to 3338.9 mm in 1990 for the period 1980–2020 in Abidjan, from 991.9 mm in 2014 to 1548.5 mm in 2007 for the period 1998–2020 in Lamto and from 866.7 mm in 2015 to 1612 mm in 2010 for the period 1990–2020 in Korhogo.

According to the classification of [40], in Abidjan, over the 41 years, 20 years are in excess while 18 years are in deficit, and 3 years have values close to the mean rainfall ( $1522 \pm 518$  mm). The AII index analysis over the studied period shows that 2020 ( $AII = +0.14$ ) is a moderately wet year, while 2018 ( $AII = -0.08$ ) and 2019 ( $AII = -0.31$ ) are moderately dry years. In Lamto, over the 23 years, 8 years are in excess, while 13 years are in deficit, and 2 years have values close to the mean rainfall ( $1229 \pm 165$  mm). The AII index analysis over the studied period revealed that 2019 ( $AII = +1.7$ ) could be considered as a strongly wet period, while 2018 ( $AII = -0.8$ ) and 2020 ( $AII = -0.8$ ) are classified as moderately dry years. Finally, in Korhogo, over the 31 years, 12 years are in excess, whereas 18 years are in deficit compared to the mean rainfall of 1187 mm, and 1 year has a value close to the mean rainfall ( $1187 \text{ mm} \pm 179$ ). AII index analysis over the studied period revealed that all three years are in deficit, with (AII) index values of  $-0.14$ ,  $-0.15$ , and  $-0.58$ , respectively, and can be considered as moderately dry periods.

### 3.2. Chemical Composition of Rainwater and Wet Deposition Fluxes

Annual Volume Weighed Mean (VWM) concentrations and Wet Deposition fluxes (WD) computed for the two-year sampling period (2019–2020) as well as Monthly Volume Weighed Mean (VWM) concentrations and Wet Deposition fluxes variation (2018–2020) along the south-north transect Abidjan-Lamto-Korhogo are presented respectively in Table A1 and in Figure S2. In Abidjan, the chemical signature of rainwater is characterized by the following ion concentrations in decreasing order:  $\text{Ca}^{2+} > \text{Cl}^- > \text{Na}^+ > \text{NH}_4^+ > \text{SO}_4^{2-} > \text{tcarb} > \text{NO}_3^- > \text{Mg}^{2+} > \text{HCOO}^- > \text{CH}_3\text{COO}^- > \text{K}^+ > \text{H}^+ > \text{C}_2\text{O}_4^{2-} > \text{C}_2\text{H}_5\text{COO}^-$ .  $\text{Ca}^{2+}$ ,  $\text{Na}^+$ ,  $\text{Cl}^-$ , and  $\text{NH}_4^+$  dominate and represent 62% of the rainwater total VWM ionic concentrations. In Lamto, VWM concentrations of ions follow a global pattern in the decreasing concentration order:  $\text{NH}_4^+ > \text{HCOO}^- > \text{Ca}^{2+} > \text{NO}_3^- > \text{CH}_3\text{COO}^- > \text{H}^+ > \text{Cl}^- > \text{Na}^+ > \text{SO}_4^{2-} > \text{Mg}^{2+} > \text{K}^+ > \text{tcarb} > \text{C}_2\text{O}_4^{2-} > \text{C}_2\text{H}_5\text{COO}^-$  and we found that  $\text{NH}_4^+$ ,  $\text{HCOO}^-$ ,  $\text{Ca}^{2+}$ , and  $\text{NO}_3^-$  are dominant, representing 55% of the total VWM ionic concentrations. In Korhogo, the general chemical

pattern in the decreasing concentration order is:  $\text{Ca}^{2+} > \text{NH}_4^+ > \text{Na}^+ > \text{HCOO}^- > \text{NO}_3^- > \text{Cl}^- > \text{K}^+ > \text{CH}_3\text{COO}^- > \text{SO}_4^{2-} > \text{H}^+ > \text{Mg}^{2+} > \text{tcarb} > \text{C}_2\text{O}_4^{2-} > \text{C}_2\text{H}_5\text{COO}^-$ .  $\text{Ca}^{2+}$ ,  $\text{NH}_4^+$ ,  $\text{Na}^+$ , and  $\text{HCOO}^-$  are found to be dominant and represent 53% of the total VWM ionic concentrations. The mean annual total ionic load is estimated to be  $191.20 \mu\text{eq L}^{-1}$ ,  $84.26 \mu\text{eq L}^{-1}$ , and  $111.75 \mu\text{eq L}^{-1}$  for Abidjan, Lamto, and Korhogo, respectively. These results demonstrate that the urban precipitations are much more loaded compared to the rural area of Lamto.

### 3.2.1. Marine Contribution

Sea-salt fractions (SSF), non-sea-salt fractions (NSSF), and enrichment factors (EF) for  $\text{K}^+$ ,  $\text{Cl}^-$ ,  $\text{Mg}^{2+}$ ,  $\text{SO}_4^{2-}$ ,  $\text{Ca}^{2+}$  ions were calculated according to the methodology outlined in (Equations (S4), (S6) and (S7)) and presented in Table A2. For the three studied sites,  $\text{Cl}^-/\text{Na}^+$  ratios were close to the sea-salt ratio of reference [39], and EFs were close to 1, showing that  $\text{Cl}^-$  is almost 100% marine, assuming that most of the sodium is from a marine source [41].  $\text{Na}^+$  and  $\text{Cl}^-$  generally originate from sea salt associated with oceanic air masses [42].  $\text{Na}^+$  and  $\text{Cl}^-$  are highly correlated ( $r = 0.94$ ;  $0.82$ ;  $0.83$ ) (Figure S1) in Abidjan, Lamto, and Korhogo, respectively, and suggest that both ions are mainly of marine origin.  $\text{Mg}^{2+}/\text{Na}^+$  ratios calculated in Abidjan and Korhogo are close to the seawater reference value, and EF values are equal to 1. This result suggests a marine origin of  $\text{Mg}^{2+}$  at Abidjan and Korhogo. This result is supported by the strong correlations coefficients calculated between  $\text{Mg}^{2+}$  and  $\text{Na}^+$ , and  $\text{Mg}^{2+}$  and  $\text{Cl}^-$ , respectively, ( $0.82$ ) and ( $0.94$ ) for Abidjan, and ( $0.64$ ) and ( $0.62$ ) for Korhogo (Figure S1).

SSF and NSSF calculations indicate that for Abidjan and Korhogo, 81% and 75% of  $\text{Mg}^{2+}$  are from a marine origin and that 19% and 25% are from non-marine sources. Lamto also presents a  $\text{Mg}^{2+}/\text{Na}^+$  ratio above the seawater reference value with an EF value close to 2, indicating an additional non-marine contribution. SSF and NSSF  $\text{Mg}^{2+}$  fractions are estimated to be 35% and 65%, respectively. In addition, we found that  $\text{Mg}^{2+}$  and  $\text{Ca}^{2+}$  are highly correlated ( $r = 0.92$ ) (Figure S1), indicating a possible terrigenous origin.  $\text{SO}_4^{2-}/\text{Na}^+$ ,  $\text{K}^+/\text{Na}^+$ , and  $\text{Ca}^{2+}/\text{Na}^+$  ratios in rainwater at all sites were found to be higher than seawater ratios values and correspond to EF values well above 1. These high ratios and EF values indicate potential contributions from anthropogenic and crustal sources in addition to the marine source [43]. SSF and NSSF calculations show that  $\text{SO}_4^{2-}$  at Abidjan, Lamto, and Korhogo is mostly of non-marine origin, with contributions of 85%, 90%, and 84%, respectively. Marine fractions for  $\text{Cl}^-$ ,  $\text{SO}_4^{2-}$ ,  $\text{K}^+$ ,  $\text{Ca}^{2+}$ , and  $\text{Mg}^{2+}$  were estimated to be approximately 94%, 15%, 13%, 3%, and 81%, respectively, at Abidjan, 92%, 10%, 5%, 2%, and 35%, respectively, at Lamto, and 100%, 16%, 3%, 2%, and 75%, respectively, at Korhogo (Table A2). The total marine contribution to the total ionic content for the three sites was computed using the following equation:

$$\text{Marine} = [\text{Na}^+] + \text{SSF}[\text{Cl}^-] + \text{SSF}[\text{Mg}^{2+}] + \text{SSF}[\text{Ca}^{2+}] + \text{SSF}[\text{K}^+] + \text{SSF}[\text{SO}_4^{2-}]. \quad (2)$$

The total marine contribution is estimated to be  $65.69 \mu\text{eq L}^{-1}$ ,  $11.59 \mu\text{eq L}^{-1}$ ,  $25.46 \mu\text{eq L}^{-1}$  representing a contribution of 34% in Abidjan, 14% in Lamto and 24% in Korhogo (Figure 3). The strong marine contribution in Abidjan is likely to be related to the coastal location of the city, resulting in a strong influence of monsoon air masses loaded with sea salt. Similar conclusions are described in several studies [44,45] where high concentrations of  $\text{Na}^+$ ,  $\text{Cl}^-$ , and  $\text{Mg}^{2+}$  were attributed to the ocean proximity. We found that Lamto records the lowest marine contribution. To analyze these results, air mass origins have been studied using back trajectory calculations from the NOAA HYSPLIT model over the study period 2017–2020 at 1500 m of altitude (Figure 4).

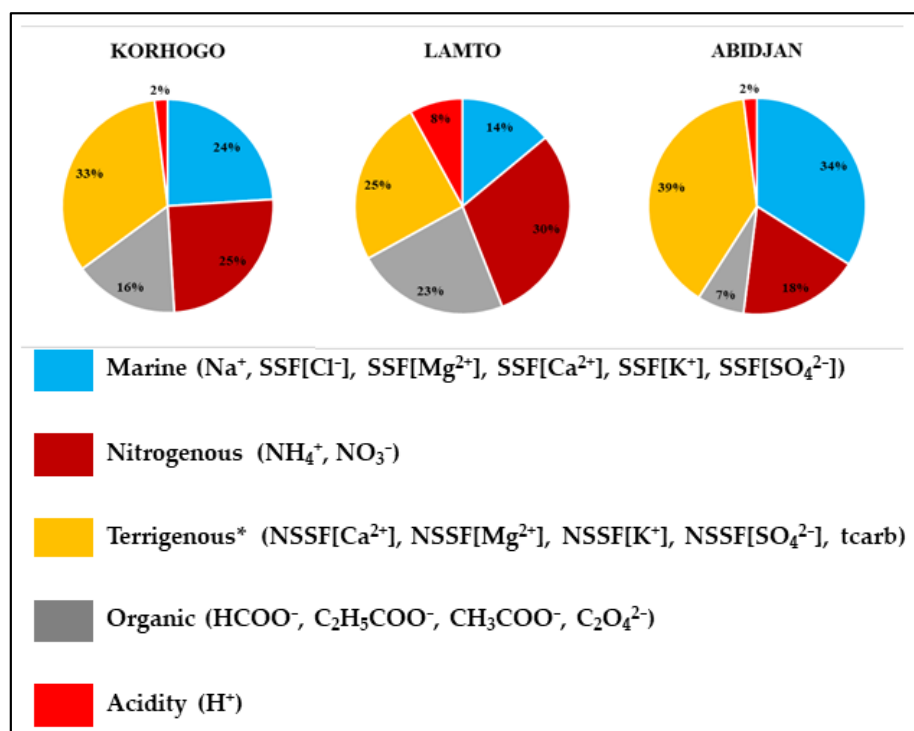


**Figure 3.** Estimation of marine, nitrogenous, terrigenous, organic, and acidity contributions to rain chemical content along the Abidjan-Lamto-Korhogo transect (\* terrigenous in this study represents a mixture of terrigenous and anthropogenic sources in urban areas, whereas in the rural Lamto site, it represents a mixture of terrigenous and biomass burning sources).

Results clearly indicate that monsoonal oceanic air masses coming from the Guinean Gulf rich in sea-salt aerosols influence Abidjan, Lamto, and Korhogo (Figure 4c,f,i). This influence is more intense in Abidjan, with a higher percentage of oceanic back trajectories (Figure 4c) compared to Lamto (Figure 4f). Despite its northernmost position and its greater distance from the coast, we found that Korhogo is significantly influenced by the marine source. Air mass back trajectories show that Korhogo is influenced both by oceanic air masses coming from the south and from the northwest border. This double contribution could explain the importance of marine source contribution in Korhogo rainfall chemical content (Figure 4i). This monsoonal oceanic influence is much greater in wet seasons than in dry seasons.

In West and Central Africa, convective rainfalls generally show a marine signature related to the boundary layer chemical content and a terrigenous signature from atmospheric levels above the boundary layer affected by continental air masses [8]. Hot and dry continental air masses originating from a high-pressure system above the Sahara Desert give rise to dusty Harmattan air masses over most of West Africa from November to February, and in summer, moist equatorial air masses originating from the Atlantic Ocean bring annual monsoon rains [46]. Our results clearly identify these two chemical signatures during the monsoon season along the studied south-north transect represented by the Abidjan, Lamto, and Korhogo sites.

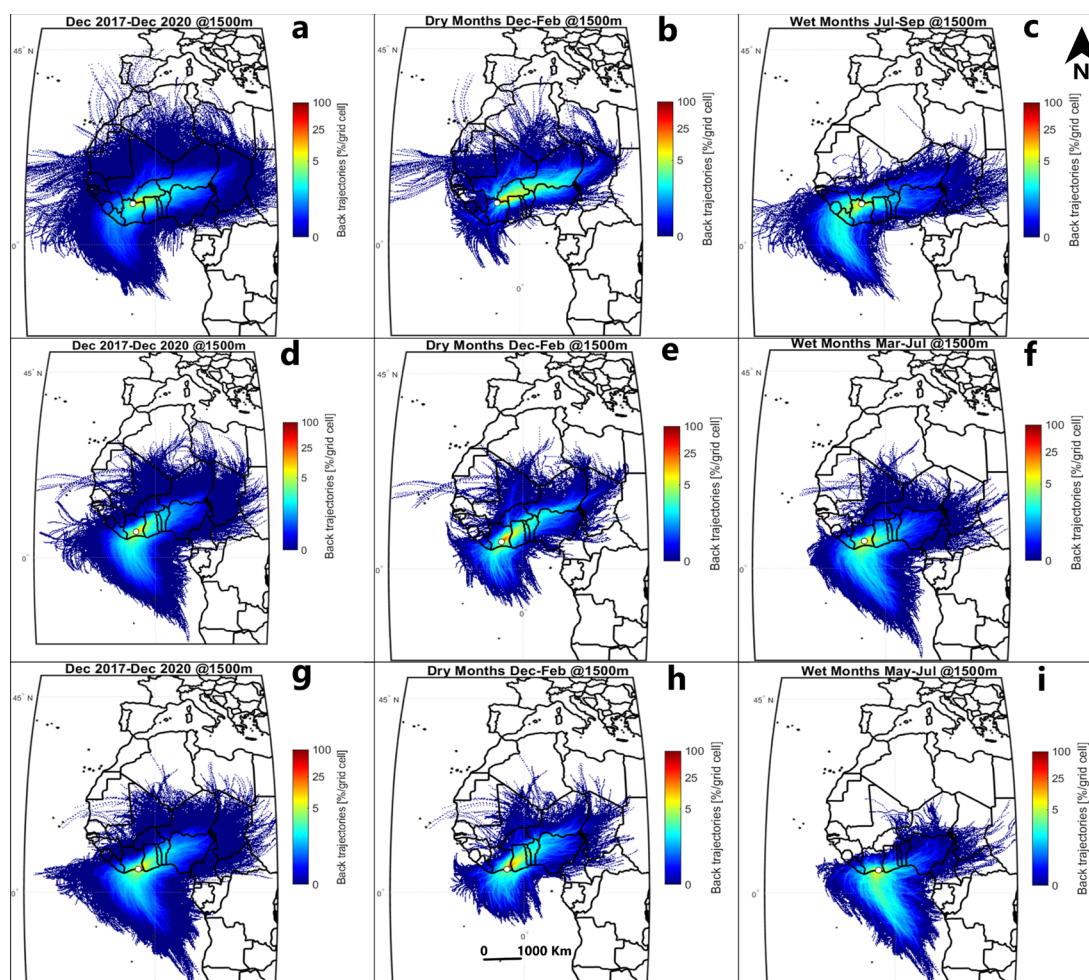


**Figure 4.** Overlay back-trajectory analyses for air masses arriving at the three sites for the study period (2017–2020) at 1500 m of altitude. (a,d,g): average back-trajectory for the whole studied period at Abidjan, Lamto, and Korhogo, respectively; (b,e,h): average dry seasons back trajectory at Abidjan (Dry months December–February), Lamto (Dry months December–February), and Korhogo (Dry months December–February), respectively. (c,f,i): average wet seasons back-trajectory at Abidjan (Wet months May–July), Lamto (Wet months March–July), and Korhogo (Wet months July–September), respectively.

### 3.2.2. Terrigenous Contribution

Table A3 presents the calculations of  $\text{SO}_4^{2-}$ ,  $\text{Mg}^{2+}$ ,  $\text{K}^+$ , and  $\text{Cl}^-$  ratios and crustal enrichment factors (EF) outlined in (Equations (S5)–(S7)) assuming that  $\text{Ca}^{2+}$  is 100% of crustal origin.  $\text{SO}_4^{2-}/\text{Ca}^{2+}$  ratio values for the three sites are higher than the reference ratio value, and their EF values are well above 1. This result confirms that  $\text{SO}_4^{2-}$  in the rain could be explained by marine, crustal, and some potential additional sources. We hypothesize that urban site rainfall at Abidjan and Korhogo could be influenced by  $\text{SO}_4^{2-}$  of anthropogenic origin.  $\text{SO}_4^{2-}$  and  $\text{NO}_3^-$  often result from anthropogenic emissions in urban areas [47], and their concentrations in the two urban sites are higher than in Lamto (Table A1). In addition, we note that Abidjan presents higher  $\text{SO}_4^{2-}$  concentrations ( $19.50 \mu\text{eq L}^{-1}$ ) compared to the other two sites. Using the ratio  $\text{SO}_4^{2-}/\text{NO}_3^-$  could allow us to distinguish mobile sources, such as traffic sources, and stationary sources, such as industry [10,48].  $\text{SO}_4^{2-}/\text{NO}_3^-$  ratio at Abidjan is 1.87, which suggests the leading role of stationary sources, e.g., industry or charcoal-burning emissions from domestic combustion [49,50]. In addition, high contents of sulfur in vehicles fuels used in West Africa and particularly in Côte d’Ivoire could explain high VWM  $\text{SO}_4^{2-}$  concentrations [51]. Bahino et al. [52] have shown that  $\text{SO}_2$  air concentration has three possible sources in Abidjan, i.e., traffic, domestic fire, and waste burning, with traffic as the main contributor.

Nevertheless,  $\text{SO}_4^{2-}$  concentration in Abidjan precipitation is lower by a factor 2 or 3 than those recorded in megacities such as Hong Kong, Jiaozhou Bay (China), and New Delhi (India) [46,53,54] (Table 2).

**Table 2.** Average Volume Weighed Mean (VWM;  $\mu\text{eq L}^{-1}$ ) concentrations in rainwater in Abidjan, Lamto and Korhogo, Côte d'Ivoire (this study) and other places in the world (adapted from [12]).

Sites	Period	n	pH	H <sup>+</sup>	Ca <sup>2+</sup>	Mg <sup>2+</sup>	Na <sup>+</sup>	K <sup>+</sup>	NH <sub>4</sub> <sup>+</sup>	HCO <sub>3</sub> <sup>-</sup>	Cl <sup>-</sup>	SO <sub>4</sub> <sup>2-</sup>	NO <sub>3</sub> <sup>-</sup>
Limeira, Brazil <sup>(a)</sup>	09/2013–03/2014	30	5.62	2.40	54.88	17.40	22.39	5.68	34.36	20.13	7.06	15.54	14.73
Jiaozhou Bay, China <sup>(b)</sup>	06/2015–05/2016	49	4.77	16.90	64.10	21.90	54.7	17.20	107.00	–	66.00	93.70	62.90
Juiz de Fora, Brazil <sup>(c)</sup>	2014	53	6.60	0.40	31.90	13.80	29.10	16.00	–	8.50	18.30	3.00	25.60
Lijiang City, China <sup>(d)</sup>	06/2012–11/2012	176	6.07	0.85	50.10	10.90	0.98	2.01	20.80	–	2.04	23.70	7.00
Djougou, Benin <sup>(e)</sup>	2006–2009	530	5.10	6.46	13.30	2.10	3.80	2.00	14.30	–	3.40	6.20	8.20
Florianópolis, Brazil <sup>(f)</sup>	08/2006–11/2006	22	4.97	10.71	7.98	9.00	59.80	3.14	–	–	56.94	9.94	15.18
Ibiúna, Brazil <sup>(g)</sup>	2006	15	6.23	0.59	114.00	10.10	37.70	8.25	56.70	–	21.20	60.90	21.80
Delhi, Índia <sup>(h)</sup>	2003–2005	355	6.39	1.02	80.88	23.11	24.35	14.18	31.81	38.42	29.52	40.81	25.17
Porto Alegre, Brazil <sup>(i)</sup>	2005–2007	177	5.30	4.98	22.40	9.28	18.40	6.48	35.30	–	16.10	22.10	3.95
Guaíba, Brazil <sup>(j)</sup>	01/2002–12/2002	70	5.72	1.90	8.41	3.85	11.10	2.81	28.10	–	6.98	13.20	2.47
Ilha Grande, Brazil <sup>(k)</sup>	03/2002–09/2002	20	5.22	6.00	9.20	40.40	142.20	7.10	9.90	–	178.20	34.80	12.00
São Paulo, Brazil <sup>(l)</sup>	01/2003–12/2003	44	5.39	4.03	21.60	6.60	8.64	9.55	37.10	–	9.29	23.80	20.10
Ankara, Turkey <sup>(m)</sup>	09/1994–12/1996	162	6.33	1.60	71.4	9.30	15.60	9.8	86.40	–	20.40	48.00	29.20
Southern Taiwan <sup>(n)</sup>	05/2005–12/2008	402	–	–	53.40	32.60	97.10	10.90	50.20	119.60	63.10	40.50	15.70
Newark, USA <sup>(o)</sup>	2006–2007	46	4.60	25.0	6.00	3.30	10.90	1.30	24.40	–	10.70	38.10	14.40
Hong Kong, China <sup>(p)</sup>	10/1998–10/2000	156	4.20	63.20	16.20	7.00	36.90	4.20	22.00	–	42.40	70	27.60
Abidjan, Côte d'Ivoire <sup>(*)</sup>	2019–2020	165	5.76	3.90	25.00	5.80	21.50	3.60	19.01	5.00	24.30	19.50	8.70
Lamto, Côte d'Ivoire <sup>(*)</sup>	2019–2020	146	5.31	6.57	9.91	2.57	5.41	2.00	17.90	1.50	5.57	4.76	7.22
Korhogo, Côte d'Ivoire <sup>(*)</sup>	2019–2020	97	5.57	4.09	20.09	3.40	11.24	8.63	17.38	2.30	9.57	5.27	9.90

n = number of samples. (a) [12], (b) [46], (c) [55], (d) [43], (e) [9], (f) [56], (g) [57], (h) [54], (i) [58], (j) [59], (k) [60], (l) [61], (m) [62], (n) [63], (o) [64], (p) [53], (\*) (this study).

Korhogo has an  $\text{SO}_4^{2-}/\text{NO}_3^-$  ratio equal to 0.58, less than 1, illustrating the relative importance of  $\text{NO}_3^-$  emissions compared to  $\text{SO}_4^{2-}$ . This result corroborates other rain chemical characteristics established at Korhogo, which is considered a moderately industrialized city. In Abidjan, the importance of anthropogenic emissions compared to the two other sites is explained by the level of population density, urbanization, and industrialization.

$\text{K}^+/\text{Ca}^{2+}$  ratios are below the reference crustal value, and EF values are above 1 for all three sites. In addition,  $\text{K}^+$  and  $\text{Ca}^{2+}$  are highly correlated (r) with values of 0.79, 0.70, and 0.73 (Figure S1), respectively, at Abidjan, Lamto, and Korhogo. These results indicate a possible terrigenous origin of  $\text{K}^+$ . The NSSF  $\text{K}^+$  fraction was found to be 87%, 96%, and 97% at Abidjan, Lamto, and Korhogo, respectively (Table A3). High correlation coefficients (r) between  $\text{Cl}^-$  and  $\text{K}^+$  with (0.75), (0.71), and (0.86) are found, respectively, at Abidjan, Lamto, and Korhogo could suggest a potential  $\text{K}^+$  origin from biomass combustion, which is known as a source of KCl [65]. Since submicronic particulate  $\text{K}^+$  is considered to be an atmospheric tracer of biomass combustion [66,67], in the urban context of Abidjan and Korhogo, we assume that the household fires burning using charcoal are a source of  $\text{K}^+$ , whereas, in Lamto, biomass burning of vegetation is likely to be the main source of  $\text{K}^+$ .

Calculations of SSF and NSSF  $\text{Mg}^{2+}$  and EFs indicate that the terrigenous contribution of this ion is limited to 19% at Abidjan and 25% at Korhogo, while it represents 65% at Lamto, with a strong correlation between  $\text{Ca}^{2+}$  and  $\text{Mg}^{2+}$  ( $r = 0.92$ ) (Table A3, Figure S1). NSSF  $\text{Ca}^{2+}$  are 97%, 98%, and 98%, respectively, at Abidjan, Lamto, and Korhogo (Table A3).  $\text{Ca}^{2+}$  displays high correlations<sup>®</sup> with  $\text{SO}_4^{2-}$  (0.86), (0.76), (0.91),  $\text{Mg}^{2+}$  (0.81), (0.92), (0.91) and  $\text{K}^+$  (0.79), (0.70), and (0.73), respectively, at Abidjan, Lamto, and Korhogo (Figure S1). We found that  $\text{Ca}^{2+}$  is the most important ion in rainwater chemical composition measured at Abidjan and Korhogo with a concentration of  $38.30 \mu\text{eq L}^{-1}$  and  $20.09 \mu\text{eq L}^{-1}$ , respectively (Table A1). At Lamto it represents the third most important ion with a concentration of  $9.91 \mu\text{eq L}^{-1}$ .  $\text{Ca}^{2+}$  predominance in the rain at the urban sites (Abidjan and Korhogo) could be explained by the contribution of multiple sources. In Abidjan, the expansion of construction activities involved cement production, which represents a potential source of  $\text{Ca}^{2+}$  particles [68–70]. In

addition, soil particle resuspension from road dust can also contribute to the precipitation  $\text{Ca}^{2+}$  content [55,71–73]. We analyzed Hysplit air mass back-trajectories at specific dates (Abidjan: 10 April 2020, Lamto: 6 March 2020, Korhogo: 28 March 2019) representative of  $\text{Ca}^{2+}$  VWM concentrations peaks of  $555 \mu\text{eq L}^{-1}$ ,  $231 \mu\text{eq L}^{-1}$  and  $164 \mu\text{eq L}^{-1}$  for Abidjan, Lamto, and Korhogo, respectively (Figure 5). At the transition between the dry and the wet season (March–April), we observe that northeast air masses coming from the Saharan desert at 2500 m of altitude heavily loaded with dust particles rich in terrigenous chemical components affect all three sites. The scavenging of these particles by rainy events at the seasonal transition explains the high VWM  $\text{Ca}^{2+}$  concentrations recorded in rainwater at the three sites at the beginning of the wet season.

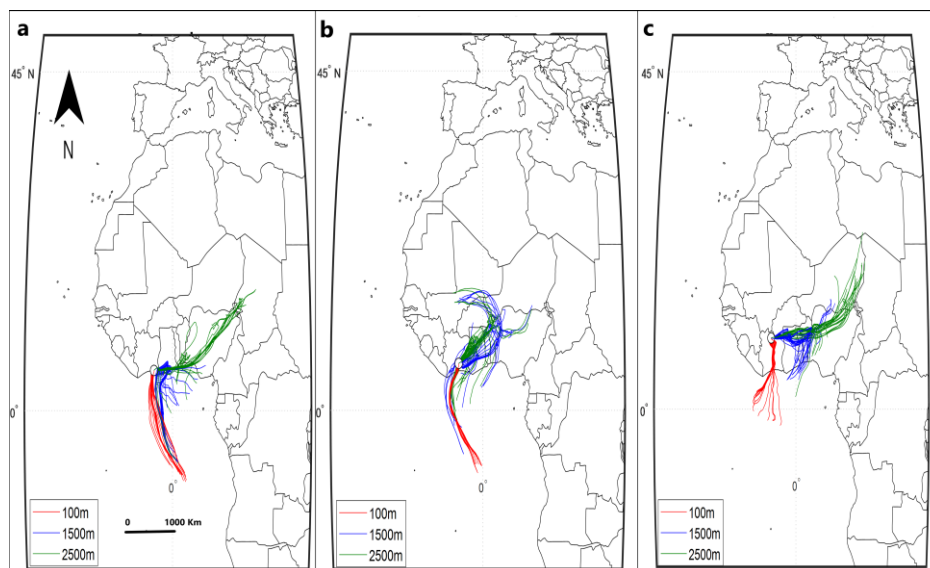


**Figure 5.** 96-h overlay back-trajectories initiated in (a) Abidjan (10 April 2020); (b) Lamto, (6 March 2020) and (c) Korhogo (28 March 2019).

The terrigenous signature identified at African sites emphasizes the direct influence of soil dust on rainfall [4]. High concentrations of calcium during the dry season are due to dust particles coming from northeast warm and dry desert air masses (Figure 4b). The North African desert areas (Sahel and Sahara) are probably the most important mineral aerosol source [74,75], and when the monsoon sets in, North East Harmattan air masses heavily loaded in soil dust terrigenous components are transported over the continent. The partial dissolution of soil dust, rain is loaded with dissolved calcium and carbonates composed of calcite, dolomite, gypsum, and also illite, smectite, or palygorskite explains the enrichment of  $\text{Ca}^{2+}$ ,  $\text{SO}_4^{2-}$ ,  $\text{Mg}^{2+}$ , and  $\text{K}^+$  in rainwater [76].

This result is similar to those obtained in other African ecosystems [1,8,9,14,77] and other regions of the world, including Asia [78]. In Korhogo, located in the northern climatic zone, we assume that  $\text{Ca}^{2+}$  terrigenous contribution is primarily related to Saharan dust transport [75] (Figure 4h). Lamto rains present the lowest total  $\text{Ca}^{2+}$  VWM concentration ( $9.91 \mu\text{eq L}^{-1}$ ) over the studied transect and the lowest terrigenous contribution. This result is in agreement with that of [15] ( $9.20 \mu\text{eq L}^{-1}$ ). Lamto, located in the climatic center zone, appeared to be less influenced by the harmattan air masses (Figure 4d,g). We compared concentrations in the rain established in Côte d’Ivoire with other results in the rest of the world (Table 2). Abidjan, Lamto, and Korhogo record a  $\text{Ca}^{2+}$  VWM concentration lower than cities such as New Delhi (India) ( $80.88 \mu\text{eq L}^{-1}$ ), Limeira (Brazil) ( $54.88 \mu\text{eq L}^{-1}$ ), and Ankara (Turkey) ( $71.40 \mu\text{eq L}^{-1}$ ) [12,54,62] but higher than those of Florianopolis, Brazil ( $7.98 \mu\text{eq L}^{-1}$ ) and Newark (USA) ( $6.00 \mu\text{eq L}^{-1}$ ) [56,64]. Our study demonstrates that highly urbanized and industrialized cities with dense demography, such as the megacity of Abidjan, will tend to have higher  $\text{Ca}^{2+}$  and  $\text{SO}_4^{2-}$  concentrations as a result of industrial activities, vehicle emissions (including road resuspension) and other emissions related to

urban activities [58]. The medium-sized city of Korhogo, less urbanized and industrialized than Abidjan, and the rural wet-savanna site of Lamto are more influenced by continental air mass transport from African deserts.

The total terrigenous contribution is estimated according to the equation:

$$\text{NSSF}[\text{Ca}^{2+}] + \text{NSSF}[\text{Mg}^{2+}] + \text{NSSF}[\text{K}^+] + \text{NSSF}[\text{SO}_4^{2-}] + \text{tcarb}. \quad (3)$$

We found a total of  $74.21 \mu\text{eq L}^{-1}$ ,  $21.61 \mu\text{eq L}^{-1}$ , and  $37.25 \mu\text{eq L}^{-1}$  that contribute to 39%, 25%, and 33% of the total ionic content, respectively, for Abidjan, Lamto, and Korhogo (Figure 3). We must specify that the so-called terrigenous contribution in this study represents a mixture of terrigenous and anthropogenic sources in urban areas, whereas, at the rural site of Lamto, it represents a mixture of terrigenous and biomass-burning sources (Figure 3). Abidjan and Korhogo present higher deposition fluxes of terrigenous ionic compounds such as calcium with annual mean WD of  $11.32 \pm 6.27 \text{ kg ha}^{-1} \text{ yr}^{-1}$  and  $4.50 \pm 2.07 \text{ kg ha}^{-1} \text{ yr}^{-1}$ , respectively.  $\text{Ca}^{2+}$  WD in Lamto is lower, with a mean annual value of  $2.59 \pm 0.31 \text{ kg ha}^{-1} \text{ yr}^{-1}$ .

### 3.2.3. Nitrogenous Contribution

The nitrogenous contribution, defined as the sum of ammonium and nitrate VWM concentrations  $[\text{NH}_4^+] + [\text{NO}_3^-]$ , is, respectively, estimated to be  $33.70 \mu\text{eq L}^{-1}$ ,  $25.12 \mu\text{eq L}^{-1}$ , and  $26.47 \mu\text{eq L}^{-1}$  and represents 18%, 30% and 25% of the total precipitation composition at Abidjan, Lamto, and Korhogo, respectively (Figure 3). Abidjan's rainfall composition exhibits the weakest nitrogenous contribution despite its highest VWM concentrations of nitrogenous species (VWM  $\text{NH}_4^+ = 22.60 \mu\text{eq L}^{-1}$  (68%) and VWM  $\text{NO}_3^- = 11.10 \mu\text{eq L}^{-1}$  (32%)). In the context of urbanization and demographic growth, the development of fossil-fuel combustion from road traffic and domestic combustion may play an important role in  $\text{NH}_3$  and  $\text{NO}_2$  emissions [79]. Similarly, [53] state that  $\text{NO}_2$  gas emissions in Abidjan have two distinct sources: (i) the limited traffic of garbage collection vehicles and the circulation of minibuses called "Gbaka", which connect the city center to the suburbs, and (ii) industrial activities. In contrast, they strongly linked  $\text{NH}_3$  gas emissions to biomass burning (firewood and charcoal) as a source of energy by most households and emissions from waste burning in Abidjan.

Lamto exhibits the highest nitrogenous contribution, representing one-third of its rainfall composition (71%  $\text{NH}_4^+$  and 29%  $\text{NO}_3^-$ ). High  $\text{NH}_4^+$  concentration could be explained by the rural features of Lamto, such as bacterial decomposition of urea in animal excreta and emissions from natural or fertilized soils by agriculture activities, which are both sources of  $\text{NH}_3$  [14,80]. As noted by [81], agricultural activity contributes to substantial  $\text{NH}_3$  gas emissions, resulting from the use of large quantities of fertilizers and plant phytosanitary products to increase rubber and cocoa harvest yields around Lamto. Savanna fires and household fuelwood burning are also primary sources of  $\text{NH}_3$  [82]. Strong correlations ( $r$ ) of  $\text{SO}_4^{2-}$  with both  $\text{NH}_4^+$  (0.72) and  $\text{NO}_3^-$  (0.77) (Figure S1) indicate that  $\text{NH}_4^+$  is related to multiphase reactions in the atmosphere. Most of the time, ammonia exists in multiple forms of aerosols in the atmosphere as  $(\text{NH}_4)_2\text{SO}_4$ ,  $\text{NH}_4\text{HSO}_4$ ,  $\text{NH}_4\text{NO}_3$ , and  $\text{NH}_4\text{F}$  [83,84]. The relatively low  $\text{NO}_3^-$  VWM concentration measured at Lamto could be explained by low biogenic  $\text{NO}_x$  emissions, according to [85]. Further, [9] propose that  $\text{NO}_3^-$  in rainwater could be the result of gas-phase transformations of  $\text{NO}_x$  to  $\text{HNO}_3$ , followed by a reaction with  $\text{NH}_3$  to form  $\text{NH}_4\text{NO}_3$ .

Nitrogenous concentration values measured at Lamto in this study for the period 2019–2020 are in the same range as those found in the study of [15] from 1995–2002, with  $17.6 \mu\text{eq L}^{-1}$  of  $\text{NH}_4^+$  and  $7.7 \mu\text{eq L}^{-1}$  of  $\text{NO}_3^-$ . The nitrogenous contribution at the Korhogo site represents the second most important contribution to the rain chemical content.  $\text{NH}_4^+$  is dominant (71%) compared to  $\text{NO}_3^-$  (29%). This result is likely related to the combined rural and urban characteristics of Korhogo, which allow a mixture of sources.  $\text{NH}_4^+$  concentrations are likely related to both the emissions of  $\text{NH}_3$  from household charcoal burning [84,86], as well as biomass burning and the use of N-fertilizer in agriculture around Korhogo [8,14,86]. Adon et al. [87] reported maximum nitrogenous gas concentrations in West and Central Africa in dry season months. Monthly mean CrIS  $\text{NH}_3$  and OMI  $\text{NO}_2$  vertical column densities (VCDs)

and MODIS burned area fraction from January 2018 to December 2020 confirm the highest  $\text{NH}_3$  and  $\text{NO}_2$  concentrations. They are related to active emission sources in the dry season at all sites, especially at Lamto, with values ranging from  $2.42 \times 10^{16}$  to  $4.53 \times 10^{17}$  molecules  $\text{NH}_3 \text{ cm}^{-1}$ ,  $1.32$  to  $12.91 \times 10^{15}$  molecules  $\text{NO}_2 \text{ cm}^{-2}$  and from 0.75 to 35.91% of the burned area burned highlighting the importance of biomass burning source in Lamto compared to the two studied urban sites (Figure S3).  $\text{SO}_4^{2-}/\text{NO}_3^-$  ratio value of 0.58 in Korhogo may indicate a substantial mobile source contribution [88]. It is worth recalling that two-wheeled vehicles are predominant in Korhogo and could be a possible source of  $\text{NO}_2$  gases [27].

VWM concentrations of nitrogenous species ( $\text{NH}_4^+$ ,  $\text{NO}_3^-$ ) measured in this study are smaller than values of cities such as Sao Paulo, Brazil ( $37.10$ ,  $20.00 \mu\text{eq L}^{-1}$ ); New Delhi, India ( $31.81$ ,  $25.17 \mu\text{eq L}^{-1}$ ) and Jiaozhou Bay, China ( $107$ ,  $62.90 \mu\text{eq L}^{-1}$ ) [46,54,61], and are slightly higher than the value of the West African rural site of Djougou in Benin ( $14.30$ ,  $8.20 \mu\text{eq L}^{-1}$ ) [9] (Table 2). Thus,  $\text{NH}_4^+$  VWM concentrations in Côte d'Ivoire and in Benin are largely lower than those recorded in urban areas such as in Brazil or in China, where urbanization, fossil fuel consumption, and intensive agriculture surroundings cities are more significant [60].

In the two rural wet savannas, INDAAF sites of Lamto in Côte d'Ivoire and Djougou in Benin, VWM  $\text{NH}_4^+$  concentrations are mainly attributed to livestock breeding, biomass burning, and, to some extent, agricultural activities [84,89]. Nitrogen is considered to be an important source of nutrients in ecosystems; however, levels above a certain critical load, which depends on the specific ecosystem, can be considered to be contributing to pollution and eutrophication of the environment [90,91]. We have computed total annual nitrogen wet deposition fluxes for the three sites, finding values of  $7.01 \text{ kgN ha}^{-1} \text{ yr}^{-1}$ ,  $4.61 \text{ kgN ha}^{-1} \text{ yr}^{-1}$ , and  $4.18 \text{ kgN ha}^{-1} \text{ yr}^{-1}$ , respectively, for Abidjan, Lamto, and Korhogo. We may conclude that nitrogen WD fluxes in the megacity of Abidjan are relatively more important than in the rural area of Lamto and in the medium city of Korhogo. In addition, we emphasize that annual nitrogen wet deposition fluxes at the three sites are dominated by  $\text{N-NH}_4^+$  with WD fluxes of  $4.68 \text{ kgN ha}^{-1} \text{ yr}^{-1}$ ,  $3.27 \text{ kgN ha}^{-1} \text{ yr}^{-1}$ , and  $2.73 \text{ kgN ha}^{-1} \text{ yr}^{-1}$ , respectively.  $\text{N-NO}_3^-$  deposition flux values are lower by a factor of two, with values of  $2.33 \text{ kgN ha}^{-1} \text{ yr}^{-1}$ ,  $1.34 \text{ kgN ha}^{-1} \text{ yr}^{-1}$ , and  $1.45 \text{ kgN ha}^{-1} \text{ yr}^{-1}$ , respectively, at Abidjan, Lamto and Korhogo. Nitrogen WD remains lower than the critical load, estimated to be  $10 \text{ kgN ha}^{-1} \text{ yr}^{-1}$ , which is defined as the highest load that will not cause chemical changes leading to long-term harmful effects on the most sensitive ecological systems [90,92]. We assess critical exceedances load-nitrogen species to measure the risk of eutrophication based on the empirical method, and we may conclude that the three sites are not exposed to potential risks for the moment. However, further investigations need to be undertaken to assess total nitrogen deposition, including both wet and dry deposition processes as well as organic nitrogen compounds [93].

#### 3.2.4. pH and Acid Contribution

Mean pH measurements for the three studied sites over the period 2018–2020 are given in Table A1, while Figure 6 presents the pH frequency distribution.

The mean pH is  $5.76 \pm 0.59$ ,  $5.31 \pm 0.32$ , and  $5.57 \pm 0.30$ , respectively, at Abidjan, Lamto, and Korhogo. Mean VWM  $\text{H}^+$  concentrations, calculated from annual mean precipitation pH, are estimated to be  $4.1 \pm 0.10 \mu\text{eq L}^{-1}$ ,  $6.57 \pm 0.04 \mu\text{eq L}^{-1}$ , and  $4.09 \pm 1.7 \mu\text{eq L}^{-1}$  at Abidjan, Lamto, and Korhogo, respectively (Table A1). The reference pH of rainwater is 5.6 representing the pure acidity of water in equilibrium with atmospheric  $\text{CO}_2$  concentration [94,95]. Acid rain is defined as rain with a pH below the threshold of 5.6 [96]. Results show that 51% of the 173 Abidjan rain events present an acidic pH lower than 5.6, while 49% have an alkaline  $\text{pH} > 5.6$ . At Lamto, precipitation is mainly acidic, with 81% of the 148 rainfall samples having a pH value below 5.6. At Korhogo, precipitation was slightly acidic, with 59% of the 83 rainfall samples having measured pH values below 5.6. This result is similar to the study of [97], where rural areas recorded higher acidity of precipitation ( $\text{pH} = 5.54 \pm 0.39$ ) compared to urban areas ( $\text{pH} = 5.77 \pm 0.26$ ). Abidjan precipitations presented a pH value comparable to cities such as Guiaba, Brazil (5.72), Lijiang City, China (6.07), and Ibuina, Brazil (6.23) [43,57,59], and Korhogo has a pH value similar to cities such as Limeira (5.62) [12]

(Table 2). In comparison to other rural ecosystems, Lamto has a pH value close to Djougou (5.10) but lower than those of Sahelian sites such as Katibougou (5.54), Dahra (6.10), and Agoufou (6.28) [4].

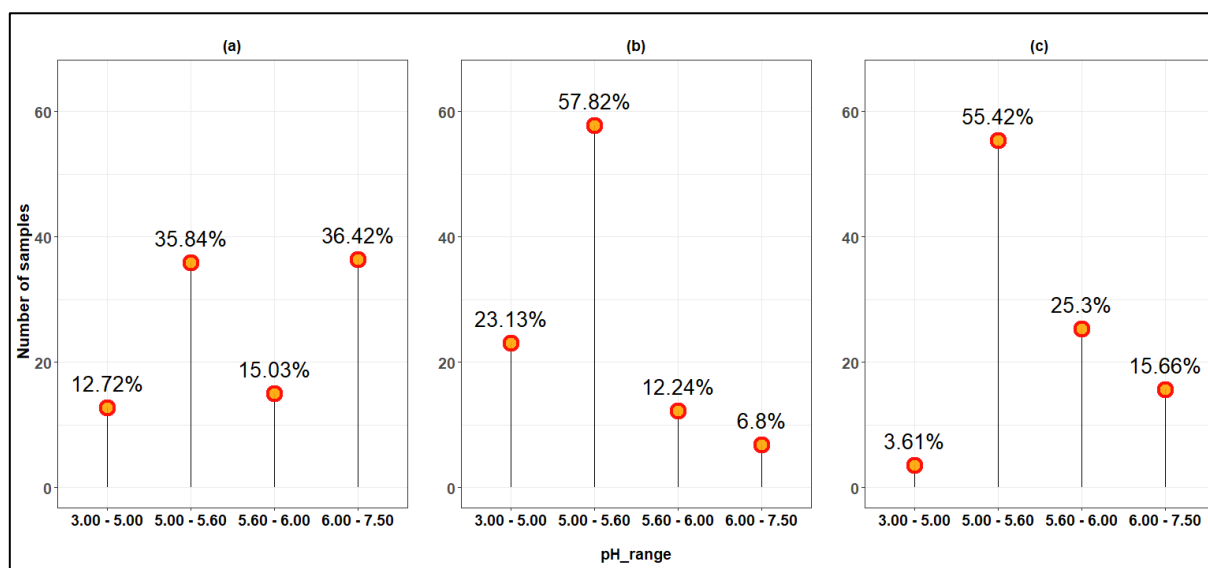


**Figure 6.** Frequency distribution of pH values of Abidjan (a), Lamto (b), and Korhogo (c) rainwater for the study period.

The electrical conductivity (EC) of rainwater relies on total soluble components, and lower EC values reflect better atmospheric environmental quality [87]. Mean EC values of precipitation measured at Abidjan, Lamto, and Korhogo ranged from 0 to 169  $\mu\text{S cm}^{-1}$ , with means of 21.36  $\mu\text{S cm}^{-1}$ , 6  $\mu\text{S cm}^{-1}$ , and 5.9  $\mu\text{S cm}^{-1}$ , respectively. Based on this observation, EC rain characteristics emphasize the lower environmental quality of Abidjan, a polluted megacity, compared to Korhogo and Lamto.

The contribution of mineral acidity, mainly related to the incorporation of  $\text{H}_2\text{SO}_4$  and  $\text{HNO}_3$ , is 69%, 38%, and 52%, respectively, at Abidjan, Lamto, and Korhogo, while organic acids represent 31%, 62%, and 48% of acidity respectively, at each site. Abidjan and Korhogo are mainly influenced by mineral acidity, whereas Lamto shows a high organic contribution. These patterns observed at urban sites are comparable to measurements made in other African ecosystems, especially in South African dry savannas influenced by anthropogenic sources [43,98].

In Figure 3, the organic contribution is computed according to the following equation:

$$[\text{HCOO}^-] + [\text{CH}_3\text{COO}^-] + [\text{C}_2\text{H}_5\text{COO}^-] + [\text{C}_2\text{O}_4^{2-}] \quad (4)$$

with values representing %, 23%, and 16% of the source's contributions to the chemical content of rainfall in Abidjan, Lamto, and Korhogo, respectively. The relatively low organic acidity in Abidjan is likely related to the fact that, in urban areas, anthropogenic activities are the main contributors to acid rain [97,99,100]. However, organic acids can be emitted in the urban environment, mainly from motorized vehicles. In the study of [101] in Abidjan, the most volatile organic compounds (VOC), which are precursors of organic acids [102], are attributed to domestic fires, landfill fires, and traffic sources. At Lamto, the high organic acidity contribution confirms results previously established by (56% organic and 44% mineral contributions) [15]. However, our study shows that the organic contribution has increased compared to the period 1995–2002 studied by [15].

The annual VWM concentration of  $\text{HCOO}^-$ ,  $\text{CH}_3\text{COO}^-$ , and  $\text{C}_2\text{O}_4^{2-}$  at Lamto are higher than at urban sites, especially for  $\text{HCOO}^-$ . The organic acidity contribution in precipitation is mainly due to VOC emissions from biomass burning and from the vegetation in rural sites [1,2,102]. Growing vegetation in the wet season produces biogenic VOC emis-

sions, which are an important source of organic acids and can explain the preponderance of  $\text{HCOO}^-$  in the wet season at Lamto. Ref. [103] found similar results in China, with the highest organic acid concentrations in the rain during the growing season (wet season) than in non-growing seasons (dry season). Despite acidity in Korhogo being dominated by mineral acidity, there is a significant contribution from organic acidity. This configuration could be related to the specificity of Korhogo, which has some rural characteristics fostering a mixture of natural sources of VOC, such as emissions from biomass burning and vegetation, and from anthropogenic sources, such as motorized vehicles.

The Neutralization Factor (NF) of mineral and organic acids by bases such as anions (oxides, carbonates, or bicarbonates, etc.) associated with base cations such as  $\text{Ca}^{2+}$ ,  $\text{NH}_4^+$ ,  $\text{Mg}^{2+}$ , and  $\text{K}^+$  can be evaluated by using Equation S9 [72,104]. Abidjan presents NF values for  $\text{Ca}^{2+}$ ,  $\text{NH}_4^+$ ,  $\text{K}^+$ , and  $\text{Mg}^{2+}$  of 0.87, 0.41, 0.10, and 0.21, respectively, revealing that  $\text{Ca}^{2+}$  is the most important ion in neutralizing acidity, followed by  $\text{NH}_4^+$ . At Korhogo and Lamto, both  $\text{Ca}^{2+}$  (NF = 0.64 and 0.32) and  $\text{NH}_4^+$  (NF = 0.57 and 0.58) ions are also the major ions that neutralize acids in rain. In Lamto,  $\text{NH}_4^+$ 's importance as the main neutralizing factor is emphasized, but strong correlations ( $r$ ) between  $\text{NH}_4^+$  and organic acids ( $\text{HCOO}^-$ ,  $\text{CH}_3\text{COO}^-$ , and  $\text{C}_2\text{O}_4^{2-}$ ), respectively, equal to 0.92, 0.90, and 0.89 (Figure S1).

According to [77], who defined Potential acidity (pA) as the sum of potential acidic compounds in the form of mineral and organic acids, we compute pAs equal to  $44.1 \mu\text{eq L}^{-1}$  at Abidjan,  $31.40 \mu\text{eq L}^{-1}$  at Lamto, and  $36.0 \mu\text{eq L}^{-1}$  at Korhogo. The measured acidity ( $4.10 \mu\text{eq L}^{-1}$ ,  $6.57 \mu\text{eq L}^{-1}$ , and  $4.09 \mu\text{eq L}^{-1}$ ) is lower by a factor of 3 to 10 compared to computed pA. In order to explain this gap, we assess the balance between neutralization and acidification processes in rainwater chemistry by using Equation S10. We computed fractional acidity (FA) to evaluate neutralizing strength of acidifying compounds [105]. Average FAs for the period (2019–2020) at Abidjan, Lamto, and Korhogo are estimated to be 0.11, 0.21, and 0.13, respectively. It indicates that 89%, 79%, and 87% of the rain acidity has been neutralized by alkaline substances at Abidjan, Lamto, and Korhogo, respectively. Consequently, neutralization processes explain the differences between potential  $\text{H}^+$  and measured acidity in precipitation collected over Côte d'Ivoire's sites.

#### 4. Conclusions

This paper documents rain chemical composition and associated wet deposition of major ionic species along a North-South transect in Côte d'Ivoire. This study presents original results over a three-year time period at two urban sites (Abidjan and Korhogo) inter-compared with a rural wet savanna site (Lamto). The mean precipitation chemical content and wet deposition fluxes are computed at the annual (2019 and 2020) and at the monthly scale for the full studied period (2018–2020). Our study emphasizes that the urban rains are much more chemically loaded compared to the rural area of Lamto, with a mean annual total ionic load estimated to be twice as high in Abidjan than in Lamto. The dominant ion at both urban sites is  $\text{Ca}^{2+}$ , whereas  $\text{NH}_4^+$  dominates the chemical content of the Lamto rural site. At Abidjan and Korhogo,  $\text{Ca}^{2+}$ ,  $\text{Na}^+$ ,  $\text{Cl}^-$ ,  $\text{NH}_4^+$  and  $\text{Ca}^{2+}$ ,  $\text{NH}_4^+$ ,  $\text{Na}^+$ , and  $\text{HCOO}^-$ , respectively, dominate the total chemical content and represent 62% and 63% of the total. The rainwater chemical signature at the rural site of Lamto is dominated by  $\text{NH}_4^+$ ,  $\text{HCOO}^-$ ,  $\text{Ca}^{2+}$ , and  $\text{NO}_3^-$  ions, representing 55% of the total. The two urban sites' rains are characterized by a terrigenous contribution characterized by a mixture of terrigenous continental and anthropogenic sources (39–33%), as well as a high marine contribution, 34% in Abidjan and 24% in Korhogo, and a significant nitrogenous contribution, 18% in Abidjan and 25% in Korhogo, mainly associated to fossil fuel from road traffic, domestic and biomass burning sources. At the rural Lamto site, marine, terrigenous, and nitrogenous contributions represent, respectively, 14%, 25%, and 30%. In addition to the high nitrogenous contribution related to biomass burning and agricultural sources, the site shows a strong organic acids component (23%) comparable to the one of Korhogo (16%). This original result has been associated with volatile organic compounds emissions from biomass burning and vegetation at the rural site and from domestic and

landfill fires and traffic at the urban sites. Mean measured pH are, respectively, 5.76, 5.31, and 5.57 for Abidjan, Lamto, and Korhogo, indicating the importance of neutralization processes in urban rainwater chemistry. We found that the acidic contribution is mainly related to mineral acidity in the urban areas, whereas it is due to organic acidity in the rural site of Lamto. Our results at the monthly scale for the three sites showed a well-marked seasonality with higher ionic load during dry seasons compared to wet seasons. Conversely, wet deposition fluxes are maximum during the wet seasons. Considering the eutrophication of the environment through rainwater, significant wet deposition fluxes of nitrogen have been estimated to be  $7.01 \text{ kgN ha}^{-1} \text{ yr}^{-1}$  (Abidjan),  $4.61 \text{ kgN ha}^{-1} \text{ yr}^{-1}$  (Lamto),  $4.18 \text{ kgN ha}^{-1} \text{ yr}^{-1}$  (Korhogo).

There is a stronger rain chemical composition contrast between the urban and rural sites than between the urban sites located in different climate zones, submitted to different rain amounts and seasonality. This could, therefore, mean that the rain content of urban sites is more likely to be determined by local emissions than large-scale and climatic influences. This unique study on rainfall composition in urban sites represents a first step toward characterizing urban deposition fluxes and understanding the composition of the atmosphere in African cities. Quantifying urban key deposition elements, such as nitrogen, is important for closing the gap in the regional budgets of ionic species, which are necessary for policymakers to manage atmospheric inputs and outputs from local ecosystems. In the future, it will be necessary to quantify total dissolved nitrogen in order to better assess eutrophication through total wet deposition of nitrogen. In addition, it is important to note that wet deposition studies should be complemented by dry deposition process evaluation to assess the global deposition budgets to improve knowledge on the biogeochemical cycle balance, soil quality, and water quality and to improve global deposition models. There is a clear need for more long-term, quality-controlled, in situ measurements in African urban areas; Africa is a key continent of the future with regard to climate and environmental issues where national and international pollutants reduction directives should be taken.

**Supplementary Materials:** The following supporting information can be downloaded at: <https://www.mdpi.com/article/10.3390/atmos14050809/s1>, Figure S1: Spearman matrix correlation of rainwater Volume Weighed Mean (VWM) concentrations ( $\mu\text{eq L}^{-1}$ ) for Abidjan, Lamto and Korhogo; Figure S2: Monthly Volume Weighed Mean (VWM) concentrations of major ions ( $\mu\text{eq L}^{-1}$ ) at Abidjan (a), Lamto (b) and Korhogo (c) and monthly Wet Deposition (WD) fluxes ( $\text{kgX ha}^{-1} \text{ yr}^{-1}$ ) at Abidjan (d), Lamto (e) and Korhogo (f); Figure S3: Monthly mean Vertical Column Densities (VCD) of  $\text{NH}_3$  from CRiS (upper panel), tropospheric VCD of  $\text{NO}_2$  from OMI (middle panel), and burned area from MODIS (lower panel) averaged over 2018–2020; S4. Calculations and Statistics [106–111].

**Author Contributions:** Conceptualization, M.L.K.-D., C.G.-L. and V.Y.; methodology, M.L.K.-D.; software, J.E.H. and K.J.; validation, C.G.-L., V.Y. and J.E.H.; formal analysis, M.L.K.-D. and E.G.; investigation, M.L.K.-D., S.G. and S.S.; resources, C.G.-L. and V.Y.; data curation, M.L.K.-D.; writing—original draft preparation, M.L.K.-D.; writing—review and editing, C.G.-L., V.Y. and C.M.-V.; visualization, M.L.K.-D., C.G.-L. and R.K.; supervision, V.Y. and C.G.-L.; project administration, V.Y. and C.G.-L.; funding acquisition, V.Y. and C.G.-L. All authors have read and agreed to the published version of the manuscript.

**Funding:** This research was funded by the Ministry of Higher Education and Research of Cote d'Ivoire, in the framework of Debt Reduction-Development Contracts (C2D) managed by the Research Institute for Development (IRD) under funding program 5768A1-PRO/PRESED-CI C2D PASMU project whose main agreement is registered under number 305984/00 within the framework of the PASMU project and also by the European Union's Horizon 2020 research and innovation program under Marie Skłodowska-Curie grant agreement No. 871944; as well as by the INDAAF programme-CNRS Centre National de la recherche Scientifique-INSU Institut National des Sciences de l'Univers-IRD Institut de Recherche pour le Développement.

**Institutional Review Board Statement:** Not applicable.

**Informed Consent Statement:** Not applicable.

**Data Availability Statement:** Raw data were collected in the framework of the PASMU project and are available on request from the coordinator Prof. V. Yoboué (veronique.yoboue94@ufhb.edu.ci). Data

of the LAMTO site are available from the INDAAF project at the address <http://indaaf.obs-mip.fr> (accessed on 26 April 2023). The pre-processed HYSPLIT trajectory data can be obtained from the corresponding author, and the trajectories can be freely calculated at the web page [https://www.ready.noaa.gov/HYSPLIT\\_traj.php](https://www.ready.noaa.gov/HYSPLIT_traj.php) (accessed on 26 April 2023). MODIS burned-area data are available from <https://doi.org/10.5067/MODIS/MCD64A1.006> (accessed on 26 April 2023) [112]. OMI L3 NO SP version 4 is available at [10.5067/MEASURES/MINDS/DATA301](https://doi.org/10.5067/MEASURES/MINDS/DATA301) (accessed on 26 April 2023) [113]. The CrIS CFPR version 1.6.3 NH<sub>3</sub> VCD data is available upon request from Environment and Climate Change Canada (mark.shephard@ec.gc.ca) [https://hpfx.collab.science.gc.ca/~mas001/satellite\\_ext/cris/snpp/nh3/v1\\_6\\_3/](https://hpfx.collab.science.gc.ca/~mas001/satellite_ext/cris/snpp/nh3/v1_6_3/) (accessed on 26 April 2023) [33].

**Acknowledgments:** This work also received a contribution from the INDAAF program, supported by the INSU/CNRS, the IRD (Institut de Recherche pour le Développement), from the Observatoire des Sciences de l'Univers EFLUVE, from the Observatoire Midi-Pyrénées. The authors would like to thank the PI and staff of the Lamto station in Côte d'Ivoire, SODEXAM (Airport, Aeronautical and Meteorological Development and Exploitation Company), EVIDENCE project (Extreme rainfall events, vulnerability to flooding and to water contamination) and finally the managers of the urban site located at the IRD within the FELIX HOUPHOUET BOIGNY University in Abidjan, and the second urban site located at the PELOFORO GON COULIBALY University (Korhogo). We thank also Enrico Dammers and Mark Shephard for their assistance with CrIS NH<sub>3</sub> data.

**Conflicts of Interest:** The authors declare no conflict of interest.

## Appendix A

**Table A1.** Annual Volume Weight Mean (VWM) ( $\mu\text{eq L}^{-1}$ ) and wet deposition fluxes (WD) ( $\text{KgX ha}^{-1} \text{yr}^{-1}$ ) in rainwater in Abidjan, Lamto and Korhogo (Côte d'Ivoire).

Species	Abidjan						Lamto						Korhogo					
	2019		2020		2019–2020		2019		2020		2019–2020		2019		2020		2019–2020	
	VWM	WD	VWM	WD	VWM	WD	VWM	WD	VWM	WD	VWM	WD	VWM	WD	VWM	WD	VWM	WD
H <sup>+</sup>	4.00	0.05	4.14	0.07	4.1 ( $\pm 0.09$ )	0.06 ( $\pm 0.01$ )	6.54	0.10	6.62	0.07	6.57 ( $\pm 0.06$ )	0.09 ( $\pm 0.02$ )	2.59	0.03	5.65	0.06	4.09 ( $\pm 2.16$ )	0.05 ( $\pm 0.02$ )
pH	5.57	-	5.89	-	5.76	-	5.24	-	5.38	-	5.31	-	5.70	-	5.40	-	5.57	-
Na <sup>+</sup>	19.00	5.93	30.95	11.34	26 ( $\pm 8.43$ )	8.8 ( $\pm 3.82$ )	4.46	1.55	6.82	1.73	5.41 ( $\pm 1.67$ )	1.62 ( $\pm 0.13$ )	16.65	4.45	2.40	0.60	11.24 ( $\pm 10.08$ )	3 ( $\pm 2.83$ )
NH <sub>4</sub> <sup>+</sup>	25.19	6.16	20.70	5.94	22.6 ( $\pm 3.18$ )	6 ( $\pm 0.15$ )	16.47	4.48	20.01	3.97	17.9 ( $\pm 2.50$ )	4.20 ( $\pm 0.36$ )	18.40	3.86	16.55	3.23	17.38 ( $\pm 1.31$ )	3.50 ( $\pm 0.54$ )
N in NH <sub>4</sub> <sup>+</sup>	19.64	4.80	16.14	4.63	17.63	4.68	12.84	3.49	15.60	3.09	13.96	3.27	14.35	3.01	12.90	2.51	13.55	2.73
K <sup>+</sup>	3.78	2.00	5.09	3.17	4.5 ( $\pm 0.93$ )	2.62 ( $\pm 0.83$ )	1.80	1.06	2.80	0.99	2 ( $\pm 0.35$ )	1.02 ( $\pm 0.05$ )	12.43	5.65	2.06	0.87	8.63 ( $\pm 7.34$ )	3.80 ( $\pm 3.52$ )
Ca <sup>2+</sup>	24.19	6.57	48.35	15.44	38.3 ( $\pm 17.08$ )	11.32 ( $\pm 6.27$ )	7.93	2.40	12.85	2.84	9.91 ( $\pm 3.48$ )	2.59 ( $\pm 0.31$ )	24.08	5.61	13.27	2.88	20.09 ( $\pm 7.64$ )	4.50 ( $\pm 2.07$ )
Mg <sup>2+</sup>	5.49	0.90	8.74	1.67	7.4 ( $\pm 2.30$ )	1.31 ( $\pm 0.55$ )	2.19	0.40	3.12	0.42	2.57 ( $\pm 0.65$ )	0.40 ( $\pm 0.01$ )	4.07	0.57	2.35	0.31	3.4 ( $\pm 1.21$ )	0.50 ( $\pm 0.20$ )
NO <sub>3</sub> <sup>-</sup>	8.79	7.39	12.77	12.62	11.1 ( $\pm 2.81$ )	10.16 ( $\pm 3.70$ )	6.26	5.86	8.63	5.89	7.22 ( $\pm 1.67$ )	5.84 ( $\pm 0.03$ )	10.72	7.73	6.97	4.68	9.09 ( $\pm 2.65$ )	6.30 ( $\pm 2.34$ )
N in NO <sub>3</sub> <sup>-</sup>	2.02	1.69	2.93	2.90	2.55	2.33	1.43	1.34	1.98	1.35	1.66	1.34	2.46	1.77	1.60	1.07	2.09	1.45
Cl <sup>-</sup>	24.40	11.74	37.44	21.18	32 ( $\pm 9.22$ )	16.77 ( $\pm 6.68$ )	4.76	2.55	7.27	2.84	5.77 ( $\pm 1.77$ )	2.67 ( $\pm 0.21$ )	13.71	5.66	2.44	0.94	9.57 ( $\pm 7.94$ )	3.80 ( $\pm 3.48$ )
SO <sub>4</sub> <sup>2-</sup>	19.49	12.69	19.38	14.83	19.5 ( $\pm 0.08$ )	13.76 ( $\pm 1.52$ )	4.24	3.07	5.54	2.93	4.76 ( $\pm 0.92$ )	2.99 ( $\pm 0.10$ )	6.01	3.35	3.84	2.00	5.27 ( $\pm 1.53$ )	2.80 ( $\pm 1.04$ )
S in SO <sub>4</sub> <sup>2-</sup>	6.43	4.18	6.39	4.89	6.43	4.50	1.39	1.01	1.82	0.96	1.57	0.98	1.98	1.10	1.26	0.66	1.73	0.92
* tCarb	7.17	2.99	17.04	16.57	12 ( $\pm 4.01$ )	11 ( $\pm 5.51$ )	2.29	1.73	3.50	1.93	2.78 ( $\pm 0.80$ )	2.21 ( $\pm 0.64$ )	5.17	0.06	2.52	0.67	4.54 ( $\pm 1.87$ )	3.10 ( $\pm 0.19$ )
HCOO <sup>-</sup>	5.57	3.48	7.76	5.70	6.80 ( $\pm 1.55$ )	4.65 ( $\pm 1.57$ )	9.74	6.76	14.12	7.16	11.51 ( $\pm 3.10$ )	6.91 ( $\pm 0.28$ )	8.71	4.66	11.18	5.57	9.97 ( $\pm 1.75$ )	5.20 ( $\pm 0.53$ )
CH <sub>3</sub> COO <sup>-</sup>	3.21	2.57	6.72	6.33	5.30 ( $\pm 2.48$ )	4.57 ( $\pm 2.66$ )	5.40	4.81	8.47	5.51	6.64 ( $\pm 2.17$ )	5.11 ( $\pm 0.49$ )	5.16	3.54	5.51	3.52	5.61 ( $\pm 0.24$ )	3.70 ( $\pm 0.10$ )
C <sub>2</sub> H <sub>5</sub> COO <sup>-</sup>	<LOD	-	<LOD	-	<LOD	-	<LOD	-	0.14	-	0.10 ( $\pm 0.04$ )	-	<LOD	-	<LOD	-	<LOD	-
C <sub>2</sub> O <sub>4</sub> <sup>2-</sup>	4.08	1.69	1.28	1.83	1.4 ( $\pm 0.24$ )	1.89 ( $\pm 0.60$ )	0.94	0.64	1.41	0.70	1.13 ( $\pm 0.33$ )	1.33 ( $\pm 0.04$ )	3.09	1.62	0.48	0.39	2.09 ( $\pm 1.85$ )	1.10 ( $\pm 0.19$ )

LOD (Limit of detection), \* tcarb = total carbonates species calculated from this equation  $tcarb = 10^{(pH-5.505)}$  [72].

**Table A2.** Seawater Enrichment Factor (EF) of  $\text{Cl}^-$ ,  $\text{SO}_4^{2-}$ ,  $\text{K}^+$ ,  $\text{Ca}^{2+}$  and  $\text{Mg}^{2+}$  in rainwater of Abidjan, Lamto and Korhogo. Calculation of marine fractions (SSF) as a percentage of the reference ratio.

Sites	Sea Water Ratios [39]	$\text{Cl}^-/\text{Na}^+$	$\text{SO}_4^{2-}/\text{Na}^+$	$\text{K}^+/\text{Na}^+$	$\text{Ca}^{2+}/\text{Na}^+$	$\text{Mg}^{2+}/\text{Na}^+$
		1.167	0.121	0.022	0.044	0.227
Abidjan	Ratios in rain	1.23	0.75	0.17	1.47	0.28
	$\text{EF}_{\text{MARINE}}$	1	6	8	33	1
	SSF (%)	94	15	13	3	81
Lamto	Ratios in rain	1.07	0.88	0.37	1.83	0.47
	$\text{EF}_{\text{MARINE}}$	1	7	17	42	2
	SSF (%)	92	10	5	2	35
Korhogo	Ratios in rain	0.85	0.47	0.77	1.79	0.3
	$\text{EF}_{\text{MARINE}}$	1	1	35	41	1
	SSF (%)	100	16	3	2	75

**Table A3.** Crustal Enrichment Factor (EF) of  $\text{Cl}^-$ ,  $\text{SO}_4^{2-}$ ,  $\text{K}^+$ ,  $\text{Ca}^{2+}$  and  $\text{Mg}^{2+}$  in rainwater of Abidjan, Lamto and Korhogo. Calculation of non-sea-salt fractions (NSSF) as a percentage of the reference ratio.

Sites	Crustal Water Ratios [39]	$\text{Cl}^-/\text{Ca}^{2+}$	$\text{SO}_4^{2-}/\text{Ca}^{2+}$	$\text{K}^+/\text{Ca}^{2+}$	$\text{Mg}^{2+}/\text{Ca}^{2+}$
		0.0031	0.0188	0.504	0.561
Abidjan	Ratios in rain	0.84	0.65	0.12	0.19
	$\text{EF}_{\text{CRUSTAL}}$	270	27	0.23	0.3
	NSSF (%)	6	85	87	19
Lamto	Ratios in rain	0.58	0.48	0.20	0.26
	$\text{EF}_{\text{CRUSTAL}}$	26	26	0.1	0.5
	NSSF (%)	8	90	96	65
Korhogo	Ratios in rain	0.44	0.93	0.28	0.61
	$\text{EF}_{\text{CRUSTAL}}$	141	49	0.26	1.1
	NSSF (%)	0	74	97	25

## References

- Galy-Lacaux, C.; Laouali, D.; Descroix, L.; Gobron, N.; Lioussé, C. Long Term Precipitation Chemistry and Wet Deposition in a Remote Dry Savanna Site in Africa (Niger). *Atmos. Chem. Phys.* **2009**, *9*, 1579–1595. [\[CrossRef\]](#)
- Vet, R.; Artz, R.S.; Carou, S.; Shaw, M.; Ro, C.-U.; Aas, W.; Baker, A.; Bowersox, V.C.; Dentener, F.; Galy-Lacaux, C.; et al. A Global Assessment of Precipitation Chemistry and Deposition of Sulfur, Nitrogen, Sea Salt, Base Cations, Organic Acids, Acidity and PH, and Phosphorus. *Atmos. Environ.* **2014**, *93*, 3–100. [\[CrossRef\]](#)
- Fu, Y.; Li, F.; Guo, S.; Zhao, M. Cadmium Concentration and Its Typical Input and Output Fluxes in Agricultural Soil Downstream of a Heavy Metal Sewage Irrigation Area. *J. Hazard. Mater.* **2021**, *412*, 125203. [\[CrossRef\]](#)
- Laouali, D.; Delon, C.; Adon, M.; Ndiaye, O.; Saneh, I.; Gardrat, E.; Dias-Alves, M.; Tagesson, T.; Fensholt, R.; Galy-Lacaux, C. Source Contributions in Precipitation Chemistry and Analysis of Atmospheric Nitrogen Deposition in a Sahelian Dry Savanna Site in West Africa. *Atmos. Res.* **2021**, *251*, 105423. [\[CrossRef\]](#)
- Rockström, J.; Steffen, W.; Noone, K.; Persson, Å.; Chapin, F.S.; Lambin, E.F.; Lenton, T.M.; Scheffer, M.; Folke, C.; Schellnhuber, H.J.; et al. A Safe Operating Space for Humanity. *Nature* **2009**, *461*, 472–475. [\[CrossRef\]](#)
- Fowler, D.; Coyle, M.; Skiba, U.; Sutton, M.A.; Cape, J.N.; Reis, S.; Sheppard, L.J.; Jenkins, A.; Grizzetti, B.; Galloway, J.N.; et al. The Global Nitrogen Cycle in the Twenty-First Century. *Philos. Trans. R. Soc. B Biol. Sci.* **2013**, *368*, 20130164. [\[CrossRef\]](#) [\[PubMed\]](#)
- Seinfeld, J.H.; Pandis, S.N. *Atmospheric Chemistry and Physics: From Air Pollution to Climate Change*; Wiley: New York, NY, USA, 1998; ISBN 978-0-471-17815-6.
- Laouali, D.; Galy-Lacaux, C.; Diop, B.; Delon, C.; Orange, D.; Lacaux, J.P.; Akpo, A.; Lavenu, F.; Gardrat, E.; Castera, P. Long Term Monitoring of the Chemical Composition of Precipitation and Wet Deposition Fluxes over Three Sahelian Savannas. *Atmos. Environ.* **2012**, *50*, 314–327. [\[CrossRef\]](#)
- Akpo, A.B.; Galy-Lacaux, C.; Laouali, D.; Delon, C.; Lioussé, C.; Adon, M.; Gardrat, E.; Mariscal, A.; Darakpa, C. Precipitation Chemistry and Wet Deposition in a Remote Wet Savanna Site in West Africa: Djougou (Benin). *Atmos. Environ.* **2015**, *115*, 110–123. [\[CrossRef\]](#)
- Keresztesi, Á.; Birsan, M.-V.; Nita, I.-A.; Bodor, Z.; Szép, R. Assessing the Neutralisation, Wet Deposition and Source Contributions of the Precipitation Chemistry over Europe during 2000–2017. *Environ. Sci. Eur.* **2019**, *31*, 50. [\[CrossRef\]](#)
- Moreda-Piñeiro, J.; Alonso-Rodríguez, E.; Moscoso-Pérez, C.; Blanco-Heras, G.; Turnes-Carou, I.; López-Mahía, P.; Muniategui-Lorenzo, S.; Prada-Rodríguez, D. Influence of Marine, Terrestrial and Anthropogenic Sources on Ionic and Metallic Composition of Rainwater at a Suburban Site (Northwest Coast of Spain). *Atmos. Environ.* **2014**, *88*, 30–38. [\[CrossRef\]](#)

12. Martins, E.H.; Nogarotto, D.C.; Mortatti, J.; Pozza, S.A. Chemical Composition of Rainwater in an Urban Area of the Southeast of Brazil. *Atmos. Pollut. Res.* **2019**, *10*, 520–530. [CrossRef]
13. Gao, Y.; Zhou, F.; Ciais, P.; Miao, C.; Yang, T.; Jia, Y.; Zhou, X.; Klaus, B.-B.; Yang, T.; Yu, G. Human Activities Aggravate Nitrogen-Deposition Pollution to Inland Water over China. *Natl. Sci. Rev.* **2020**, *7*, 430–440. [CrossRef]
14. Galy-Lacaux, C.; Modi, A.I. Precipitation Chemistry in the Sahelian Savanna of Niger, Africa. *J. Atmos. Chem.* **1998**, *30*, 319–343. [CrossRef]
15. Yoboué, V.; Galy-Lacaux, C.; Lacaux, J.P.; Silué, S. Rainwater Chemistry and Wet Deposition over the Wet Savanna Ecosystem of Lamto (Côte d’Ivoire). *J. Atmos. Chem.* **2005**, *52*, 117–141. [CrossRef]
16. United Nations, Department of Economic and Social Affairs Population Dynamics. *UN World Urban Population World Urbanization Prospects the 2011 Revision*; United Nations: New York, NY, USA, 2011.
17. United Nations, Department of Economic and Social Affairs. *Population Division World Population Prospects: The 2017 Revision, Key Findings and Advance Tables*; Working Paper No. ESA/P/WP/248; United Nations: New York, NY, USA, 2017.
18. World Bank. *World Bank Towards Environmentally Sustainable Development in Sub-Saharan Africa*. In *Africa Region Findings & Good Practice Infobriefs*; No. 78.; World Bank: Washington, DC, USA, 2017.
19. World Meteorological Organization. *State of the Climate in Africa 2020*; WMO-No. 1275; World Meteorological Organization: Geneva, Switzerland, 2021.
20. Gnamien, S.; Yoboué, V.; Liousse, C.; Osohou, M.; Keita, S.; Bahino, J.; Siélé, S.; Diaby, L. Particulate Pollution in Korhogo and Abidjan (Cote d’Ivoire) during the Dry Season. *Aerosol Air Qual. Res.* **2021**, *21*, 200201. [CrossRef]
21. INS, Institut National de Statistique. *RPGH2014, 2014, Recensement Général de la Population et l’Habitat, Rapport d’Exécution et Présentation des Principaux Résultats*. Available online: <https://www.ins.ci/> (accessed on 26 April 2023).
22. Keita, S.; Liousse, C.; Assamoi, E.-M.; Doumbia, T.; N’Datchoh, E.T.; Gnamien, S.; Elguindi, N.; Granier, C.; Yoboué, V. African Anthropogenic Emissions Inventory for Gases and Particles from 1990 to 2015. *Earth Syst. Sci. Data* **2021**, *13*, 3691–3705. [CrossRef]
23. Yao, K.; Echui, A. Desiré, Renouveau du Parc Automobile et Développement Durable en Côte D’ivoire. In *Proceedings of the Conférence CODATU XVII-Mobilité Intelligente, Inclusive et Soutenable Mobilité Intelligente, Inclusive et Soutenable* Hyderabad (Inde), Hyderabad, India, 4–6 November 2017.
24. Kouadio, K.Y.; Ali, K.E.; Zahiri, E.P.; Assamoi, A.P. Etude de La Prédicibilité de La Pluviométrie En Côte d’Ivoire Durant La Période de Juillet à Septembre. *Rev. Ivoir. Des Sci. Technol.* **2007**, *10*, 117–134.
25. Bassett, T.J. Le Boom de l’anacarde Dans Le Bassin Cotonnier Du Nord Ivoirien: Structures de Marché et Prix à La Production. *Afr. Contemp.* **2018**, *263264*, 59–83. [CrossRef]
26. Sangare, N.; Doho, B.T.A.; Kouakou, B.; Koffi, B.É. Urban Dynamics and Governance of Peri-Urban Neighbourhoods in the City of Korhogo (Côte d’Ivoire) from 2002 to 2020. *Revue de Géographie Tropicale et d’Environnement*, *1*, 2021. *EDUCI* **2021**.
27. Roger, D.M.; Abou, D.; Denis, H.K.; Koffi, B.É. Émergence De Taxi-Motos Et Recomposition SpatioÉconomique À Korhogo: Les Taxi-Villes Entre Stratégies D’adaptation Et Désespoir. *Eur. Sci. J. ESJ* **2016**, *12*, 190. [CrossRef]
28. Gautier, L. Contact Forêt-Savane En Côte d’Ivoire Centrale: Evolution de La Surface Forestiere de La Reserve de Lamto (Sud Du V-Baoule.) Candoella, *Bulletin de la Société Botanique de France. Actual. Bot.* **1989**, *136*, 85–92.
29. Diawara, A.; Yoroba, F.; Kouadio, K.Y.; Kouassi, K.B.; Assamoi, E.M.; Diedhiou, A.; Assamoi, P. Climate Variability in the Sudano-Guinean Transition Area and Its Impact on Vegetation: The Case of the Lamto Region in Côte D’Ivoire. *Adv. Meteorol.* **2014**, *2014*, 831414. [CrossRef]
30. World Meteorological Organization. *Global Atmosphere Watch Manual for the Gaw Precipitation Chemistry Programme Guidelines, Data Quality Objectives and Standard Operating Procedures No 160.*; WMO: Geneva, Switzerland, 2004.
31. Shephard, M.W.; Cady-Pereira, K.E. Cross-Track Infrared Sounder (CrIS) Satellite Observations of Tropospheric Ammonia. *Atmos. Meas. Tech.* **2015**, *8*, 1323–1336. [CrossRef]
32. Shephard, M.W.; Dammers, E.; Cady-Pereira, K.E.; Kharol, S.K.; Thompson, J.; Gainariu-Matz, Y.; Zhang, J.; McLinden, C.A.; Kovachik, A.; Moran, M.; et al. Ammonia Measurements from Space with the Cross-Track Infrared Sounder: Characteristics and Applications. *Atmos. Chem. Phys.* **2020**, *20*, 2277–2302. [CrossRef]
33. Krotkov, N.A.; Lamsal, L.N.; Celarier, E.A.; Swartz, W.H.; Marchenko, S.V.; Bucsela, E.J.; Chan, K.L.; Wenig, M.; Zara, M. The Version 3 OMI NO<sub>2</sub> Standard Product. *Atmospheric Meas. Tech.* **2017**, *10*, 3133–3149. [CrossRef]
34. Draxler, R.R.; Hess, G.D. *Description of the HYSPLIT-4 Modeling System*. NOAA Technical Memorandum ERL ARL-224; NOAA Air Resources Laboratory: Silver Spring, MD, USA, 1997; pp. 1–24.
35. Kok, L.; Van Zyl, P.G.; Beukes, J.P.; Swartz, J.S.; Burger, R.P.; Ellis, S.; Josipovic, M.; Vakkari, V.; Laakso, L.; Kulmala, M. Chemical Composition of Rain at a Regional Site on the South African Highveld. *Water SA* **2021**, *47*, 326–337. [CrossRef]
36. Kouadio, Y.K.; Ochou, D.A.; Servain, J. Tropical Atlantic and Rainfall Variability in Côte d’Ivoire. *Geophys. Res. Lett.* **2003**, *30*, CLI5-1. [CrossRef]
37. Goula, B.T.; Srohourou, B.; Brida, A.; N’zué, K.A.; Goroza, G. Determination and Variability of Growing Seasons in Cote d’Ivoire. *Int. J. Eng. Sci.* **2010**, *2*, 5993–6003.
38. Leroux, M. *The Meteorology and Climate of Tropical Africa*. In *Springer-Praxis Books in Environmental Sciences*; Springer: Chichester, UK, 2001; ISBN 978-1-85233-643-1.
39. Keene, W.C.; Pszenny, A.A.P.; Galloway, J.N.; Hawley, M.E. Sea-Salt Corrections and Interpretation of Constituent Ratios in Marine Precipitation. *J. Geophys. Res.* **1986**, *91*, 6647. [CrossRef]

40. Sarr, M.A. Évolution Récente du Climat et de la Végétation au Sénégal: Cas du Bassin Versant du Ferlo. Ph.D. Thesis, Université Jean Moulin, Lyon, France, 2009.
41. Cao, Y.-Z.; Wang, S.; Zhang, G.; Luo, J.; Lu, S. Chemical Characteristics of Wet Precipitation at an Urban Site of Guangzhou, South China. *Atmos. Res.* **2009**, *94*, 462–469. [[CrossRef](#)]
42. Niu, H.; He, Y.; Zhu, G.; Xin, H.; Du, J.; Pu, T.; Lu, X.; Zhao, G. Environmental Implications of the Snow Chemistry from Mt. Yulong, Southeastern Tibetan Plateau. *Quat. Int.* **2013**, *313*, 168–178. [[CrossRef](#)]
43. Conradie, E.H.; Van Zyl, P.G.; Pienaar, J.J.; Beukes, J.P.; Galy-Lacaux, C.; Venter, A.D.; Mkhathshwa, G.V. The Chemical Composition and Fluxes of Atmospheric Wet Deposition at Four Sites in South Africa. *Atmos. Environ.* **2016**, *146*, 113–131. [[CrossRef](#)]
44. Hoinaski, L.; Franco, D.; Haas, R.; Martins, R.F.; Lisboa, H.d.M. Investigation of Rainwater Contamination Sources in the Southern Part of Brazil. *Environ. Technol.* **2014**, *35*, 868–881. [[CrossRef](#)]
45. Xing, J.; Song, J.; Yuan, H.; Li, X.; Li, N.; Duan, L.; Qu, B.; Wang, Q.; Kang, X. Chemical Characteristics, Deposition Fluxes and Source Apportionment of Precipitation Components in the Jiaozhou Bay, North China. *Atmos. Res.* **2017**, *190*, 10–20. [[CrossRef](#)]
46. Nicholson, S.E. The West African Sahel: A Review of Recent Studies on the Rainfall Regime and Its Interannual Variability. *ISRN Meteorol.* **2013**, *2013*, 453521. [[CrossRef](#)]
47. Keresztesi, Á.; Nita, I.-A.; Boga, R.; Birsan, M.-V.; Bodor, Z.; Szép, R. Spatial and Long-Term Analysis of Rainwater Chemistry over the Conterminous United States. *Environ. Res.* **2020**, *188*, 109872. [[CrossRef](#)]
48. Xu, Z.; Wu, Y.; Liu, W.-J.; Liang, C.-S.; Ji, J.; Zhao, T.; Zhang, X. Chemical Composition of Rainwater and the Acid Neutralizing Effect at Beijing and Chizhou City, China. *Atmos. Res.* **2015**, *164*, 278–285. [[CrossRef](#)]
49. Li, C.; Li, S.-L.; Yue, F.-J.; He, S.-N.; Shi, Z.-B.; Di, C.-L.; Liu, C.-Q. Nitrate Sources and Formation of Rainwater Constrained by Dual Isotopes in Southeast Asia: Example from Singapore. *Chemosphere* **2020**, *241*, 125024. [[CrossRef](#)]
50. Naimabadi, A.; Shirmardi, M.; Maleki, H.; Teymouri, P.; Goudarzi, G.; Shahsavani, A.; Sorooshian, A.; Babaei, A.A.; Mehrabi, N.; Baneshi, M.M.; et al. On the Chemical Nature of Precipitation in a Populated Middle Eastern Region (Ahvaz, Iran) with Diverse Sources. *Ecotoxicol. Environ. Saf.* **2018**, *163*, 558–566. [[CrossRef](#)]
51. Marc, G.; Marietta, H.; Andreas, M.; Gian-Valentino, V. Dirty Diesel. *Public Eye* **2016**, *355*, i6726.
52. Bahino, J.; Yoboué, V.; Galy-Lacaux, C.; Adon, M.; Akpo, A.; Keita, S.; Lioussé, C.; Gardrat, E.; Chiron, C.; Ossouhou, M.; et al. A Pilot Study of Gaseous Pollutants' Measurement (NO<sub>2</sub>, SO<sub>2</sub>, NH<sub>3</sub>, HNO<sub>3</sub> and O<sub>3</sub>) in Abidjan, Côte d'Ivoire: Contribution to an Overview of Gaseous Pollution in African Cities. *Atmos. Chem. Phys.* **2018**, *18*, 5173–5198. [[CrossRef](#)]
53. Wai, K.M.; Tanner, P.A.; Tam, C.W.F. 2-Year Study of Chemical Composition of Bulk Deposition in a South China Coastal City: Comparison with East Asian Cities. *Environ. Sci. Technol.* **2005**, *39*, 6542–6547. [[CrossRef](#)] [[PubMed](#)]
54. Tiwari, S.; Kulshrestha, U.C.; Padmanabhamurthy, B. Monsoon Rain Chemistry and Source Apportionment Using Receptor Modeling in and around National Capital Region (NCR) of Delhi, India. *Atmos. Environ.* **2007**, *41*, 5595–5604. [[CrossRef](#)]
55. Mimura, A.M.S.; Almeida, J.M.; Vaz, F.A.S.; de Oliveira, M.A.L.; Ferreira, C.C.M.; Silva, J.C.J. Chemical Composition Monitoring of Tropical Rainwater during an Atypical Dry Year. *Atmos. Res.* **2016**, *169*, 391–399. [[CrossRef](#)]
56. Hoinaski, L.; Franco, D.; Stuetz, R.M.; Sivret, E.C.; de Melo Lisboa, H. Investigation of PM<sub>10</sub> Sources in Santa Catarina, Brazil through Graphical Interpretation Analysis Combined with Receptor Modelling. *Environ. Technol.* **2013**, *34*, 2453–2463. [[CrossRef](#)]
57. Conceição, F.T.d.; Sardinha, D.d.S.; Navarro, G.R.B.; Antunes, M.L.P.; Angelucci, V.A. Composição Química Das Águas Pluviais e Deposição Atmosférica Anual Na Bacia Do Alto Sorocaba (SP). *Quím. Nova* **2011**, *34*, 610–616. [[CrossRef](#)]
58. Migliavacca, D.; Teixeira, E.; Wiegand, F.; Machado, A.; Sanchez, J. Atmospheric Precipitation and Chemical Composition of an Urban Site, Guaíba Hydrographic Basin, Brazil. *Atmos. Environ.* **2005**, *39*, 1829–1844. [[CrossRef](#)]
59. Migliavacca, D.M.; Teixeira, E.C.; Rodriguez, M.T.R. Composição Química Da Precipitação Úmida Da Região Metropolitana de Porto Alegre, Brasil, 2005-2007. *Quím. Nova* **2012**, *35*, 1075–1083. [[CrossRef](#)]
60. Souza, P.A.; Mello, W.Z.; Maldonado, J.; Evangelista, H. Composição Química Da Chuva e Aporte Atmosférico Na Ilha Grande, RJ. *Quím. Nova* **2006**, *29*, 471–476. [[CrossRef](#)]
61. Fontenele, A.P.G.; Pedrotti, J.J.; Fornaro, A. Avaliação de Metais Traços e Íons Majoritários Em Águas de Chuva Na Cidade de São Paulo. *Quím. Nova* **2009**, *32*, 839–844. [[CrossRef](#)]
62. Topçu, S.; Incecik, S.; Atımtay, A.T. Chemical Composition of Rainwater at EMEP Station in Ankara, Turkey. *Atmos. Res.* **2002**, *65*, 77–92. [[CrossRef](#)]
63. Tsai, Y.I.; Hsieh, L.-Y.; Kuo, S.-C.; Chen, C.-L.; Wu, P.-L. Seasonal and Rainfall-Type Variations in Inorganic Ions and Dicarboxylic Acids and Acidity of Wet Deposition Samples Collected from Subtropical East Asia. *Atmos. Environ.* **2011**, *45*, 3535–3547. [[CrossRef](#)]
64. Song, F.; Gao, Y. Chemical Characteristics of Precipitation at Metropolitan Newark in the US East Coast. *Atmos. Environ.* **2009**, *43*, 4903–4913. [[CrossRef](#)]
65. Lara, L.B.L.S.; Artaxo, P.; Martinelli, L.A.; Victoria, R.L.; Camargo, P.B.; Krusche, A.; Ayers, G.P.; Ferraz, E.S.B.; Ballester, M.V. Chemical Composition of Rainwater and Anthropogenic Influences in the Piracicaba River Basin, Southeast Brazil. *Atmos. Environ.* **2001**, *35*, 4937–4945. [[CrossRef](#)]
66. Andreae, M.O.; Andreae, T.W.; Annegarn, H.; Beer, J.; Cachier, H.; Le Canut, P.; Elbert, W.; Maenhaut, W.; Salma, I.; Wienhold, F.G.; et al. Airborne Studies of Aerosol Emissions from Savanna Fires in Southern Africa: 2. Aerosol Chemical Composition. *J. Geophys. Res. Atmos.* **1998**, *103*, 32119–32128. [[CrossRef](#)]

67. de Mello, W.Z. Precipitation Chemistry in the Coast of the Metropolitan Region of Rio de Janeiro, Brazil. *Environ. Pollut.* **2001**, *114*, 235–242. [[CrossRef](#)]
68. Shakya, K.M.; Peltier, R.E.; Shrestha, H.; Byanju, R.M. Measurements of TSP, PM<sub>10</sub>, PM<sub>2.5</sub>, BC, and PM Chemical Composition from an Urban Residential Location in Nepal. *Atmos. Pollut. Res.* **2017**, *8*, 1123–1131. [[CrossRef](#)]
69. Samara, C.; Tsitouridou, R. Fine and Coarse Ionic Aerosol Components in Relation to Wet and dry Deposition. *Water. Air. Soil Pollut.* **2000**, *120*, 71–88. [[CrossRef](#)]
70. Khwaja, H.A.; Husain, L. Chemical Characterization of Acid Precipitation in Albany, New York. *Atmos. Environ. Part Gen. Top.* **1990**, *24*, 1869–1882. [[CrossRef](#)]
71. Fernandes, A.M. Características Hidrogeoquímicas da Bacia de Drenagem do Rio Sorocaba, SP: Processos Erosivos Mecânicos e Químicos. Doutorado em Química na Agricultura e no Ambiente. Ph.D. Thesis, Universidade de São Paulo, Piracicaba, Brazil, 2012.
72. Kulshrestha, U.C.; Kulshrestha, M.J.; Sekar, R.; Sastry, G.S.R.; Vairamani, M. Chemical Characteristics of Rainwater at an Urban Site of South-Central India. *Atmos. Environ.* **2003**, *37*, 3019–3026. [[CrossRef](#)]
73. Riccio, A.; Chianese, E.; Tirimerio, G.; Prati, M.V. Emission Factors of Inorganic Ions from Road Traffic: A Case Study from the City of Naples (Italy). *Transp. Res. Part Transp. Environ.* **2017**, *54*, 239–249. [[CrossRef](#)]
74. Kaufman, Y.J. Dust Transport and Deposition Observed from the Terra-Moderate Resolution Imaging Spectroradiometer (MODIS) Spacecraft over the Atlantic Ocean. *J. Geophys. Res.* **2005**, *110*, D10S12. [[CrossRef](#)]
75. Marticorena, B.; Chatenet, B.; Rajot, J.L.; Traoré, S.; Coulibaly, M.; Diallo, A.; Koné, I.; Maman, A.; NDiaye, T.; Zakou, A. Temporal Variability of Mineral Dust Concentrations over West Africa: Analyses of a Pluriannual Monitoring from the AMMA Sahelian Dust Transect. *Atmos. Chem. Phys.* **2010**, *10*, 8899–8915. [[CrossRef](#)]
76. Avila, A.; Queralt-Mitjans, I.; Alarcón, M. Mineralogical Composition of African Dust Delivered by Red Rains over Northeastern Spain. *J. Geophys. Res. Atmos.* **1997**, *102*, 21977–21996. [[CrossRef](#)]
77. Sigha-Nkamdjou, L.; Galy-Lacaux, C.; Pont, V.; Richard, S.; Sighomnou, D.; Lacaux, J.P. Rainwater Chemistry and Wet Deposition over the Equatorial Forested Ecosystem of Zoétélé (Cameroon). *J. Atmos. Chem.* **2003**, *46*, 173–198. [[CrossRef](#)]
78. Tiwari, S.; Hopke, P.K.; Thimmaiah, D.; Dumka, U.C.; Srivastava, A.K.; Bisht, D.S.; Rao, P.S.P.; Chate, D.M.; Srivastava, M.K.; Tripathi, S.N. Nature and Sources of Ionic Species in Precipitation across the Indo-Gangetic Plains, India. *Aerosol Air Qual. Res.* **2016**, *16*, 943–957. [[CrossRef](#)]
79. Ehrnsperger, L.; Klemm, O. Source Apportionment of Urban Ammonia and Its Contribution to Secondary Particle Formation in a Mid-Size European City. *Aerosol Air Qual. Res.* **2021**, *21*, 200404. [[CrossRef](#)]
80. Schlesinger, W.H.; Hartley, A.E. A Global Budget for Atmospheric NH<sub>3</sub>. *Biogeochemistry* **1992**, *15*, 191–211. [[CrossRef](#)]
81. N’goran, A.S. Agriculture Traditionnelle Et Échecs Des Politiques De Gestion Des Aires Protégées En Côte d’Ivoire: Le Cas De La Réserve De Lamto. *Eur. Sci. J. ESJ* **2016**, *12*, 209. [[CrossRef](#)]
82. Delmas, R.; Lacaux, J.P.; Menaut, J.C.; Abbadie, L.; Le Roux, X.; Helas, G.; Lobert, J. Nitrogen Compound Emission from Biomass Burning in Tropical African Savanna FOS/DECAFE 1991 Experiment (Lamto, Ivory Coast). *J. Atmos. Chem.* **1995**, *22*, 175–193. [[CrossRef](#)]
83. Seinfeld, J.H. Atmospheric Chemistry and Physics of Air Pollution. In *A Wiley Interscience Publication*; Wiley: New York, NY, USA, 1986; ISBN 978-0-471-82857-0.
84. Zhang, M.; Wang, S.; Wu, F.; Yuan, X.; Zhang, Y. Chemical Compositions of Wet Precipitation and Anthropogenic Influences at a Developing Urban Site in Southeastern China. *Atmos. Res.* **2007**, *84*, 311–322. [[CrossRef](#)]
85. Serça, D.; Delmas, R.; Le Roux, X.; Parsons, D.A.B.; Scholes, M.C.; Abbadie, L.; Lensi, R.; Ronce, O.; Labroue, L. Comparison of Nitrogen Monoxide Emissions from Several African Tropical Ecosystems and Influence of Season and Fire. *Glob. Biogeochem. Cycles* **1998**, *12*, 637–651. [[CrossRef](#)]
86. Dentener, F.J.; Crutzen, P.J. A Three-Dimensional Model of the Global Ammonia Cycle. *J. Atmos. Chem.* **1994**, *19*, 331–369. [[CrossRef](#)]
87. Adon, M.; Galy-Lacaux, C.; Yoboué, V.; Delon, C.; Lacaux, J.P.; Castera, P.; Gardrat, E.; Pienaar, J.; Al Ourabi, H.; Laouali, D.; et al. Long Term Measurements of Sulfur Dioxide, Nitrogen Dioxide, Ammonia, Nitric Acid and Ozone in Africa Using Passive Samplers. *Atmos. Chem. Phys.* **2010**, *10*, 7467–7487. [[CrossRef](#)]
88. Rao, W.; Han, G.; Tan, H.; Jin, K.; Wang, S.; Chen, T. Chemical and Sr Isotopic Characteristics of Rainwater on the Alxa Desert Plateau, North China: Implication for Air Quality and Ion Sources. *Atmos. Res.* **2017**, *193*, 163–172. [[CrossRef](#)]
89. Ossouhou, M.; Galy-Lacaux, C.; Yoboué, V.; Adon, M.; Delon, C.; Gardrat, E.; Konaté, I.; Ki, A.; Zouzou, R. Long-Term Atmospheric Inorganic Nitrogen Deposition in West African Savanna over 16 Year Period (Lamto, Côte d’Ivoire). *Environ. Res. Lett.* **2020**, *16*, 015004. [[CrossRef](#)]
90. Bobbink, R.; Hicks, K.; Galloway, J.; Spranger, T.; Alkemade, R.; Ashmore, M.; Bustamante, M.; Cinderby, S.; Davidson, E.; Dentener, F.; et al. Global Assessment of Nitrogen Deposition Effects on Terrestrial Plant Diversity: A Synthesis. *Ecol. Appl.* **2010**, *20*, 30–59. [[CrossRef](#)]
91. Josipovic, M.; Annegarn, H.J.; Kneen, M.A.; Pienaar, J.J.; Piketh, S.J. Atmospheric Dry and Wet Deposition of Sulphur and Nitrogen Species and Assessment of Critical Loads of Acidic Deposition Exceedance in South Africa. *S. Afr. J. Sci.* **2011**, *107*, 10. [[CrossRef](#)]

92. Nilsson, J. Critical Loads for Sulphur and Nitrogen. In *Air Pollution and Ecosystems*; Mathy, P., Ed.; Springer: Dordrecht, The Netherlands, 1988; pp. 85–91. ISBN 978-94-010-8276-1.
93. Bakayoko, A.; Galy-Lacaux, C.; Yoboué, V.; Hickman, J.E.; Roux, F.; Gardrat, E.; Julien, F.; Delon, C. Dominant Contribution of Nitrogen Compounds in Precipitation Chemistry in the Lake Victoria Catchment (East Africa). *Environ. Res. Lett.* **2021**, *16*, 045013. [[CrossRef](#)]
94. Charlson, R.J.; Rodhe, H. Factors Controlling the Acidity of Natural Rainwater. *Nature* **1982**, *295*, 683–685. [[CrossRef](#)]
95. Galloway, J.N.; Likens, G.E.; Keene, W.C.; Miller, J.M. The Composition of Precipitation in Remote Areas of the World. *J. Geophys. Res.* **1982**, *87*, 8771. [[CrossRef](#)]
96. Drever, J.I. *The Geochemistry of Natural Waters: Surface and Groundwater Environments*, 3rd ed.; Prentice Hall: Upper Saddle River, NJ, USA, 1997; ISBN 978-0-13-272790-7.
97. Payus, C.M.; Jikilim, C.; Sentian, J. Rainwater Chemistry of Acid Precipitation Occurrences Due to Long-Range Transboundary Haze Pollution and Prolonged Drought Events during Southwest Monsoon Season: Climate Change Driven. *Heliyon* **2020**, *6*, e04997. [[CrossRef](#)] [[PubMed](#)]
98. Mphepya, J.N.; Pienaar, J.J.; Galy-Lacaux, C.; Held, G.; Turner, C.R. Precipitation Chemistry in Semi-Arid Areas of Southern Africa: A Case Study of a Rural and an Industrial Site. *J. Atmos. Chem.* **2004**, *47*, 1–24. [[CrossRef](#)]
99. Radojevic, M.; Harrison, R.M. *Atmospheric Acidity: Sources, Consequences, and Abatement*; Elsevier Applied Science: New York, NY, USA, 1992; ISBN 978-1-85166-777-2.
100. Park, S.-M.; Seo, B.-K.; Lee, G.; Kahng, S.-H.; Jang, Y. Chemical Composition of Water Soluble Inorganic Species in Precipitation at Shihwa Basin, Korea. *Atmosphere* **2015**, *6*, 732–750. [[CrossRef](#)]
101. Dominutti, P.; Keita, S.; Bahino, J.; Colomb, A.; Lioussé, C.; Yoboué, V.; Galy-Lacaux, C.; Morris, E.; Bouvier, L.; Sauvage, S.; et al. Anthropogenic VOCs in Abidjan, Southern West Africa: From Source Quantification to Atmospheric Impacts. *Atmos. Chem. Phys.* **2019**, *19*, 11721–11741. [[CrossRef](#)]
102. Guenther, A.; Karl, T.; Harley, P.; Wiedinmyer, C.; Palmer, P.I.; Geron, C. Estimates of Global Terrestrial Isoprene Emissions Using MEGAN (Model of Emissions of Gases and Aerosols from Nature). *Atmos. Chem. Phys.* **2006**, *6*, 3181–3210. [[CrossRef](#)]
103. Niu, Y.; Li, X.; Pu, J.; Huang, Z. Organic Acids Contribute to Rainwater Acidity at a Rural Site in Eastern China. *Air Qual. Atmos. Health* **2018**, *11*, 459–469. [[CrossRef](#)]
104. Possanzini, M.; Buttini, P.; Di Palo, V. Characterization of a Rural Area in Terms of Dry and Wet Deposition. *Sci. Total Environ.* **1988**, *74*, 111–120. [[CrossRef](#)]
105. Balasubramanian, R.; Victor, T.; Chun, N. Chemical and Statistical Analysis of Precipitation in Singapore. *Water. Air. Soil Pollut.* **2001**, *130*, 451–456. [[CrossRef](#)]
106. Chao, C.Y.; Wong, K.K. Residential indoor PM10 and PM2.5 in Hong Kong and the elemental composition. *Atmospheric Environ.* **2002**, *36*, 265–277. [[CrossRef](#)]
107. Keene, W.C.; Galloway, J.N. Considerations regarding sources for formic and acetic acids in the troposphere. *J. Geophys. Res. Atmos.* **1986**, *91*, 14466. [[CrossRef](#)]
108. Safai, P.; Rao, P.; Momin, G.; Ali, K.; Chate, D.; Praveen, P. Chemical composition of precipitation during 1984–2002 at Pune, India. *Atmos. Environ.* **2004**, *38*, 1705–1714. [[CrossRef](#)]
109. Celle-Jeanton, H.; Travi, Y.; Loÿe-Pilot, M.-D.; Huneau, F.; Bertrand, G. Rainwater chemistry at a Mediterranean inland station (Avignon, France): Local contribution versus long-range supply. *Atmos. Res.* **2009**, *91*, 118–126. [[CrossRef](#)]
110. Rastogi, N.; Sarin, M. Chemical characteristics of individual rain events from a semi-arid region in India: Three-year study. *Atmos. Environ.* **2005**, *39*, 3313–3323. [[CrossRef](#)]
111. Lu, X.; Li, L.Y.; Li, N.; Yang, G.; Luo, D.; Chen, J. Chemical characteristics of spring rainwater of Xi’an city, NW China. *Atmos. Environ.* **2011**, *45*, 5058–5063. [[CrossRef](#)]
112. Giglio, L.; Loboda, T.; Roy, D.P.; Quayle, B.; Justice, C.O. An Active-Fire Based Burned Area Mapping Algorithm for the MODIS Sensor. *Remote Sens. Environ.* **2009**, *113*, 408–420. [[CrossRef](#)]
113. Lamsal, L.N.; Krotkov, N.A.; Celarier, E.A.; Swartz, W.H.; Pickering, K.E.; Bucsela, E.J.; Gleason, J.F.; Martin, R.V.; Philip, S.; Irie, H.; et al. Evaluation of OMI Operational Standard NO<sub>2</sub> Column Retrievals Using in Situ and Surface-Based NO<sub>2</sub> Observations. *Atmos. Chem. Phys.* **2014**, *14*, 11587–11609. [[CrossRef](#)]

**Disclaimer/Publisher’s Note:** The statements, opinions and data contained in all publications are solely those of the individual author(s) and contributor(s) and not of MDPI and/or the editor(s). MDPI and/or the editor(s) disclaim responsibility for any injury to people or property resulting from any ideas, methods, instructions or products referred to in the content.